FINAL REPORT: DOE PROJECT NO. DE-FG-26-99-BC15185

Award Dates: September 20, 1999 through September 19, 2000

Report Date: January 13, 2006

Gypsy Field Project in Reservoir Characterization

Submitted by:

Dr. John P. Castagna
Dr. William J. Lamb
Dr. Carlos Moreno
Dr. Roger Young
Dr. Lynn Soreghan
The University of Oklahoma
School of Geology and Geophysics
100 East Boyd Street, SEC 810
Norman, OK 73019
Tel: (405) 325-3253; Fax: (405) 325-3140

Administrative Contact:

Ms. Jennie I. Parker, Sponsored Programs Coordinator
Office of Research Services
The University of Oklahoma
731 Elm Avenue, Room 134
Norman, OK 73019
E-Mail: gradora1@ou.edu
Tel: (405) 325-6054; Fax: (405) 325-6029

Applicable University of Oklahoma Identifiers: DUNS Number 848348348, CAGE Code 3G168
The University of Oklahoma is registered as a vendor in the Central Contractor Registry (CCR).

FINAL REPORT: DOE PROJECT NO. DE-FG-26-99-BC15185
Dr. John P. Castagna

TABLE OF CONTENTS

Abstract-Gypsy Field Project in Reservoir Characterization

The objective of the Gypsy Project was to properly calculate seismic attributes and integrate these into a reservoir characterization project. Significant progress was made on the project in four areas.

1) Attenuation: In order for seismic inversion for rock properties or calculation of seismic attributes used to estimate rock properties to be performed validly, it is necessary to deal with seismic data that has had true amplitude and frequency content restored to account for earth filtering effects that are generally not included in seismic reservoir characterization methodologies. This requires the accurate measurement of seismic attenuation, something that is rarely achieved in practice. It is hoped that such measurements may also provide additional independent seismic attributes for use in reservoir characterization studies. In 2000, we were concerned with the ground truthing of attenuation measurements in the vicinity of wells. Our approach to the problem is one of extracting as time varying wavelet and relating temporal variations in the wavelet to an attenuation model of the earth. This method has the advantage of correcting for temporal variations in the reflectivity spectrum of the earth which confound the spectral ratio methodology which is the most commonly applied means of measuring attenuation from surface seismic data. Part I of the report describes our efforts in seismic attenuation as applied to the Gypsy data.

2) Optimal Attributes: A bewildering array of seismic attributes is available to the reservoir geoscientist to try to establish correlations to rock properties. Ultimately, the use of such a large number of degrees of freedom in the search for correlations with limited well control leads to common misapplication of statistically insignificant results which yields invalid predictions. Cross-validation against unused wells can be used to recognize such problems, but does not offer a solution to the question of which attributes should be used to make predictions other than by exhaustive trial and error. Alternatively, we use the approach of using principle component analysis to reduce the seismic data to a minimum number of significant attributes that explain the variation in the data. These are then correlated to rock properties in order to make predictions. Part II of the report describe our efforts in optimal attributes as applied to the Gypsy data.

High Resolution 3D Seismic Processing: When faced with the issue of testing the above methods on the Gypsy dataset, we realized that the 3D seismic data were not processed well and exhibited poor ties to well control. The data was reprocessed with surface consistent predictive deconvolution, muting of wide-angle reflections, min/max exclusion stacking, and F-XY deconvolution. After reprocessing, a good character match with synthetic seismograms was observed. This work was presented at the 2001 SEG Annual Meeting and is included as Part III of this report.

Reservoir Characterization Education: The Gypsy project has provided the data for a reservoir characterization module which was added to Depositional Systems and Stratigraphy, a course required for majors in Geology and Geophysics. This module is important because it introduces students to the relevance of sedimentary geology to applied, real-world problems. This work was presented at the Geological Society of America annual meeting (Part IV) and is described on the website for the course (Part V of the report).

Introduction

In a previous report (Lamb, 1998A) the importance of attenuation for seismic studies was discussed. Two areas that a better understanding of attenuation would impact were discussed. First, the velocities derived from sonic logs, obtained at tens of kilohertz, could be related to the velocities at tens of Hertz, which are observed on seismic data. Second, there is the possibility that information about fluid flow properties (specifically the ratio of permeability to viscosity) might be obtained from seismic data if attenuation could be understood and measured.

The Gypsy Field data were considered to be a good candidate for testing theories of attenuation in the field because of the availability of a wide variety of data: Well logs, 3D surface seismic, VSP's etc. Most important, however, was the fact that the 3D seismic data were of high frequency content and very good bandwidth. This would be critical for interpreting attenuation, which is inherently a frequency dependent effect.

One reason for the high frequency content was that the area where the well log and seismic data could be compared was the near surface (~ 1400 ft or .3 sec). In this region the seismic energy would not travel far enough to lose much frequency content. Dynamite sources were used, so frequencies of up to ~200 Hz. are useable.

While working with the near surface is good for frequency content, it has its disadvantages. Normally, in seismic work, the target area is many thousands of feet deep. This influences decisions on all phases of seismic work: seismic acquisition and processing, well logs and algorithms for synthetic seismograms. It turns out that many things which work quite well for deep targets are less appropriate shallow ones.

In our first quick look (Lamb, 1998), these issues were ignored. We proceeded with the log and seismic data as provided, and used conventional algorithms for synthetic seismograms. Not surprisingly, the ties between synthetic seismograms and seismic data were poor. Of course, we were not the first to notice this (Seifert 1994). At that point the problem could have been well logs, synthetic seismogram or wavelet extraction algorithms, or seismic data. It is now clear that all three play a part. Our attempt to address all of these is discussed below in the first part of this report.

Looking beyond the attenuation studies, the Gypsy data provide an avenue to explore new ways to do quantitative interpretation of (stacked) seismic data, especially of relating the seismic response to geological models of reservoir intervals. To approach this task, we define a set of optimal (in a sense defined below) attributes which quantify the information in the seismic. This knowledge of the information content of the seismic data is incorporated into geological models which are used to calibrate the relation between geology and seismic response, and provide the framework for inversion. Progress along this path is provided in the second part of this report.

Part I: Absorption and Attenuation

The key to obtaining information about attenuation is to extract the wavelet. The wavelet is the filter which relates well log data to seismic data. Attenuation studies proceed by examining the frequency content of the wavelet as time (and depth) vary. Because it is a necessary preliminary, and all problems have not yet been solved, we will focus here on extracting the wavelet. The areas of concern for wavelet extraction are well logs, algorithms, and seismic data. They will be addressed in that order.

Well Logs

In a naïve wavelet extraction only two well logs are needed: sonic and density. Both contribute to the reflection coefficients, while only the sonic contributes to time to depth conversion. In a more sophisticated analysis, many logs will affect the reflection coefficients and both sonic and density will affect the time to depth conversion.

The sonic will be addressed first both because of its importance, and the poor quality of the logs. Well 5-7 was chosen for special attention since it was near the center of the area of the seismic survey, where the fold was highest and the seismic data quality presumptively the highest.

The full waveform sonic log was of very poor quality. For about 40% of the logged interval the compressional flag indicated bad data. Most of the bad data was in the top half of the logged range, but about 30 feet of bad data are just below the Gypsy interval. The original sonic is shown in Figure 1.

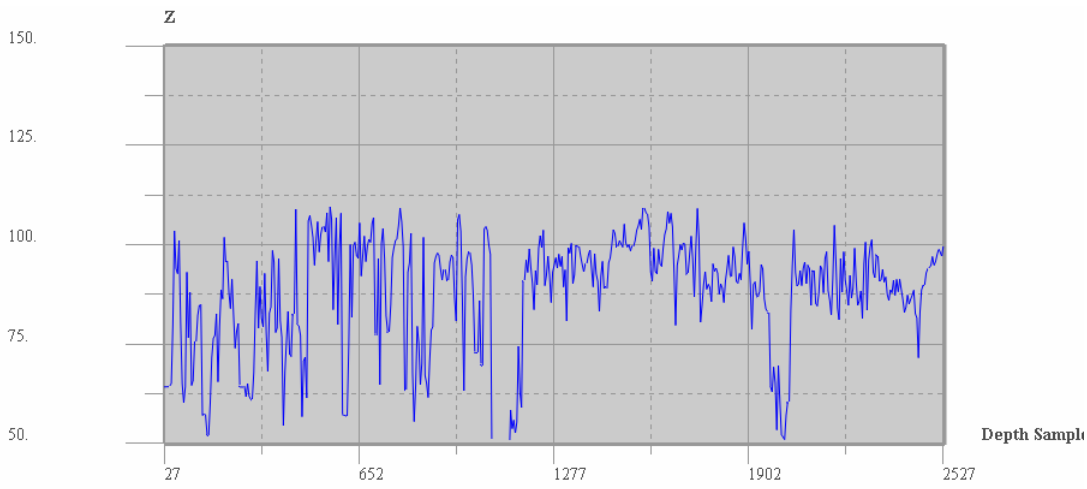

Figure 1. Original sonic log for well 5-7. The X axis is depth samples which correspond to depths 67 –1300 ft. The Y axis is transit time in microseconds / ft.

Even a brief inspection indicates that much of the upper half of the log gives much too small transit times.

Editing 40% of a log is normally extremely difficult. Fortunately, there are two factors in our favor. First, there are many nearby wells with good logs. Secondly, close examination of repeat sections and other wells shows that the algorithm for picking velocities often picked the compressional velocity as the shear velocity. The bulk of the sonic log editing consisted in replacing sections of the original compressional sonic with pieces of the original shear sonic. This problem is, of course, unique to the sonic log.

There are two problems with the borehole that affect all the logs to some degree. First, there is a change of bit size from 14 ¾ to 9 7/8 at 620 ft. Then there are washouts – many in the region above 620 ft, and just below the bit size change from 634-642 ft. Comparison with well 11-7 is most useful for this zone, since the corresponding geology is shifted by about 15 ft relative to the bit size change. The edited sonic is shown in Figure 2.

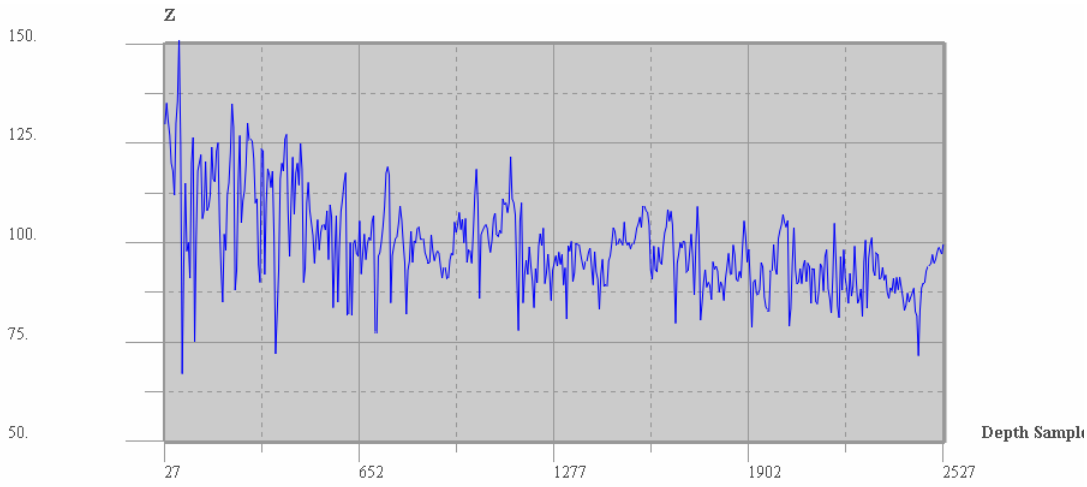

Figure 2. Edited sonic log for well 5-7. The X axis is depth samples which correspond to depths 67 –1300 ft. The Y axis is transit time in microseconds / ft. These sacles are the same as Figure 1.

This is a tremendous change from the original sonic log. Note especially that there are only occasional small transit times in the upper half of the log. The remaining small transit times are very likely real. They correlate between wells, and comparison with other logs in the same well indicate carbonate streaks. Two results of these changes are worth noting: the edit below the Gypsy interval removes a strong but spurious event from the region of greatest interest, and the large number of changes in the upper half will give much greater times for a given depth.

Moreno (2000) has edited the sonic logs for wells 1-7, 7-7 and 9-7 using the same philosophy. None of them needed to be edited to the extent of well 5-7. Sonic logs for wells 8-7 and 11-7 were deemed good enough not need editing.

Next, the bulk density is edited. The original log is shown in Figure 3.

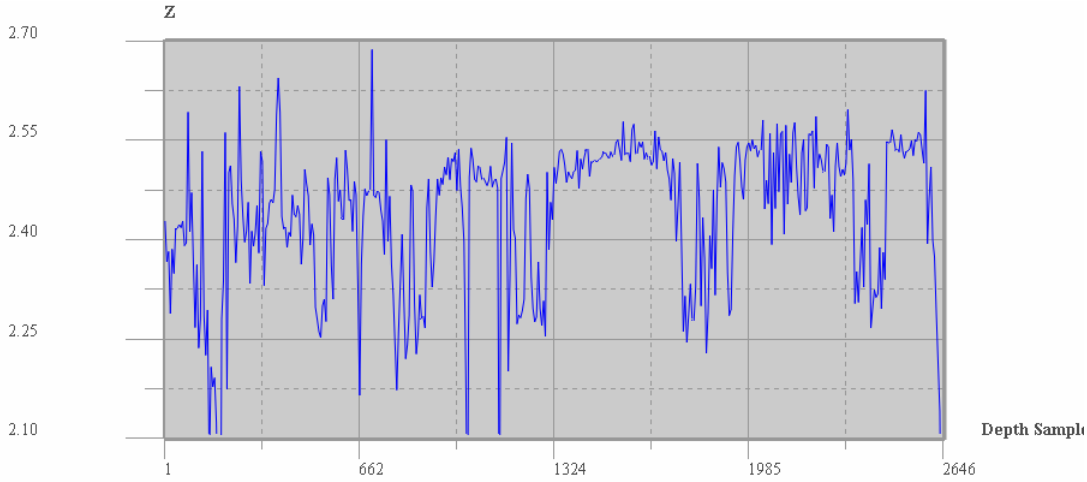

Figure3. Original bulk density log for well 5-7. The X axis is depth samples which correspond to depths 55 –1377 ft. The Y axis is transit time in microseconds / ft.

There are occasional spikes of low density due to washouts. The edited log is shown in Figure 4.

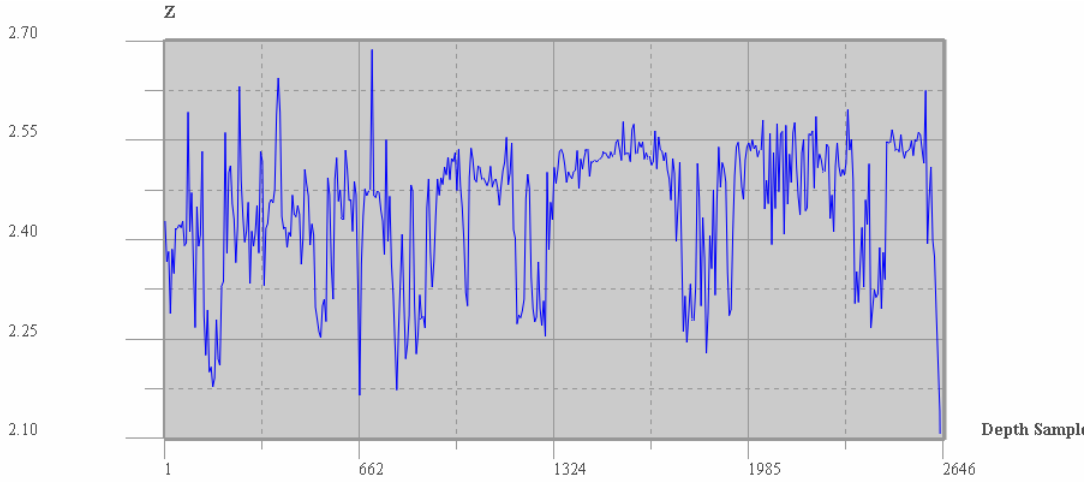

Figure 4. Edited bulk density log for well 5-7. The X axis is depth samples which correspond to depths 55 –1377 ft. The Y axis is transit time in microseconds / ft.

The sonic and density logs suffice for normal incidence synthetic seismograms. However, the area of interest is very shallow (surface to ~1400 ft or ~ .3 sec), so the range of relevant incidence angles will be large and angle dependent reflectivity may be important. To address this possibility shear velocities are needed. Now the full

waveform sonic does provide a shear log, which is in fact of poor quality. In fact, as we have seen, in many places the nominal shear log picks the compressional velocity.

Given the poor quality of the shear log, it is more reliable to estimate the shear velocity from the compressional velocity via a trend curve. Greatest accuracy can be obtained using trend curves that depend on lithology. To provide this will require a lithology analysis, which in turn will require that the neutron porosity and photoelectric effect logs also be edited. These edits are similar to those of the bulk density – repairing a few zones that suffer from washouts.

Synthetic Seismograms

Stacked Sections and Angle Dependent Reflectivity

Seismic experiments involve complicated poroelastic wave propagation. Ultimately, we are not interested in this process, but rather in a model of the material properties (density, velocities) of the subsurface. Relating the results of a seismic experiment to the underlying material properties can, in principle, be done in many ways. At one extreme, one could take a material properties model, do a complete numerical solution to the appropriate wave equation, and compare the results with the raw seismic data. At the other extreme, seismic data can be processed to be as close as possible to the geology. This is what has traditionally been done.

The convolutional model for synthetic seismograms assumes that processed (stacked) seismic data may be represented as the convolution of a time series of reflection coefficients R with a wavelet W:

$$S(i) = \sum_j R(i-j)\ W(j) \qquad (1A)$$

In the simplest view the reflection coefficients are those of a normal incidence plane wave. They are given by

$$R(i) = (\rho(i)\ V(i) - \rho(i-1)\ V(i-1)) / (\rho(i)\ V(i) + \rho(i-1)\ V(i-1)) \qquad (1B)$$

Where V is the compressional velocity for P waves incident and reflected, or the shear velocity for S waves. The reflection coefficients are zero for normal incidence converted waves.

There many things processing must do to make seismic data conform to equation 1. Only primary reflections are kept. Surface waves, head waves, multiple reflections etc. are eliminated. Effects of spherical spreading, absorption and transmission losses are compensated for. Finally, the incoming and outgoing signals must be made to conform to plane waves at normal incidence.

For many cases, the biggest approximation is taking the reflection coefficients to be those for normal incidence. The most common seismic section is the "stack " in which reflections at the same spatial position but with different incidence angles are summed. Ideally, this gives

$$\text{Stack}(i) = \sum_j \{\sum_o R(\theta(o); i-j)\} W(j) \qquad (2)$$

Where the θ's are the incidence angles. They depend on the source / receiver geometry and the velocity distribution. The second sum is over the offset o between source and receiver. The reflection coefficients as a function of angle (for isotropic media) may be determined exactly from Zöppritz Equations (Young and Braile, 1976). Equation 2 is a convolutional model, where the reflection coefficients R in equation 1 are replaced by the term in brackets in equation 2.

A very high quality estimate of the reflection coefficients for a stack may be produced by estimating the incidence angles using ray tracing, and summing the Zöppritz responses for those angles. The ray-tracing should account for short period multiple effects, tracing the path of the "effective", not the true primary. This is discussed in detail in Appendix A.

Because the Zöppritz solutions are analytically complicated they are often approximated in the form (e.g. Zheng, 1991) for small angles (typically < 30 degrees)

$$R(\theta) = A + B\ SIN^2(\theta) \qquad (3A)$$

for incident and reflected waves of the same type (P or S). For converted waves the corresponding form is

$$R(\theta) = A\ SIN(\theta) + B\ SIN^3(\theta) \qquad (3B)$$

For large angles the exact Zöppritz results are not easily approximated by expansions of the form (3) even when additional terms are used. (See e.q. Grant and West, 1965, p. 57)

Using (3), the stack can then be approximated by

$$\text{Stack}(i) = \sum_\theta \{A(i) + B(i) \sin^2(\theta)\} \qquad (4A)$$

For P or S waves, and

$$\text{Stack}(i) = \sum \{A\ \sin(\theta) + B \sin^3(\theta)\} \qquad (4B)$$

for converted waves.

Sometimes the seismic processing attempts to produce A and B sections. When this is the case, ties to well logs are made using equation 1 with the reflection coefficients for the chosen angle ranges.

To get a feel for the importance of angle dependent effects for our data, we ray traced through the velocity / density model for well 5-7. Ten offsets ranged from 100 ft. to 1200 ft. The results are shown in Figure 5:

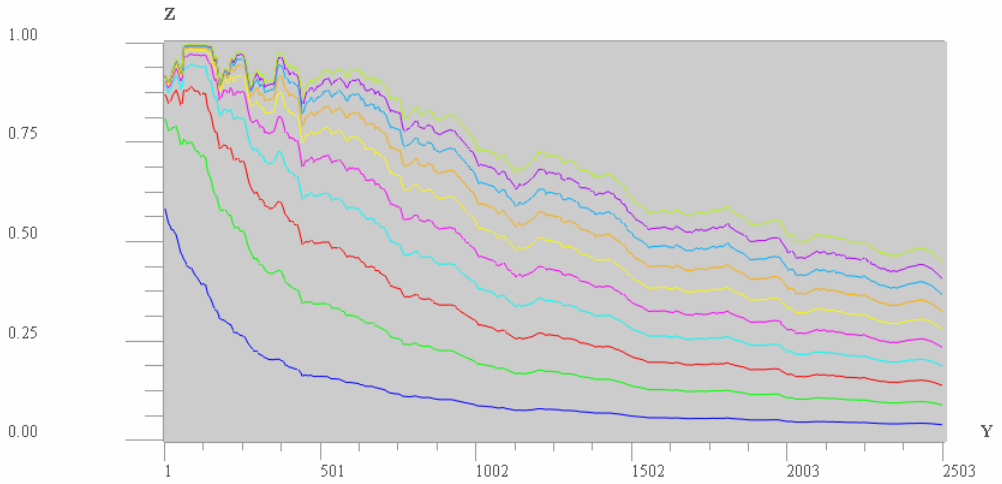

Figure 5. Sin of the incidence angle versus depth at well 5-7 for 10 offsets. The x axis is the depth sample corresponding to approximately 67.5 ft. to 1318.5 ft. The y axis is the sin of the incidence angle. The 10 offsets range from 100 ft. to 1200 ft. 10 Ft is blue, 1200ft. is light green.

Note that even for the conservative choice of 1200 ft. for the maximum offset, for much of the relevant depth, some of the farther offsets have incidence angles exceeding 30 degrees ($\sin(\theta) > .5$). So not only is angle dependence likely to be important, but the small angle approximations to Zöppritz are likely to be inadequate.

Comparison of zero offset and full Zöppritz reflections show the importance of angle dependence. Figure 6 shows the normal incidence reflection coefficients, while figure 7 shows the real part of the full Zöppritz reflection coefficients.

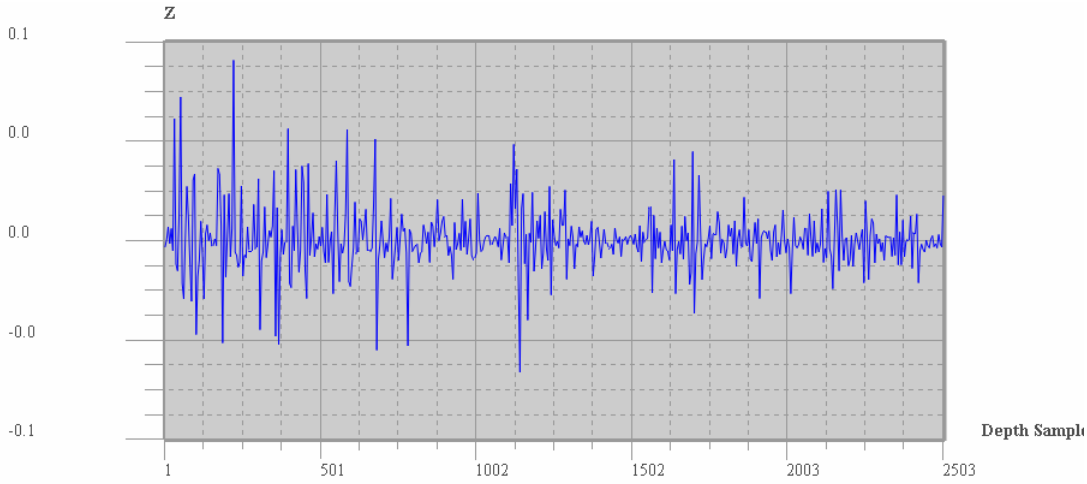

Figure 6. Normal incidence reflection coefficients for well 5-7. The x axis is the depth sample number, corresponding to depths from 67.5 ft. to 1318.5ft. The y axis is the reflection coefficient.

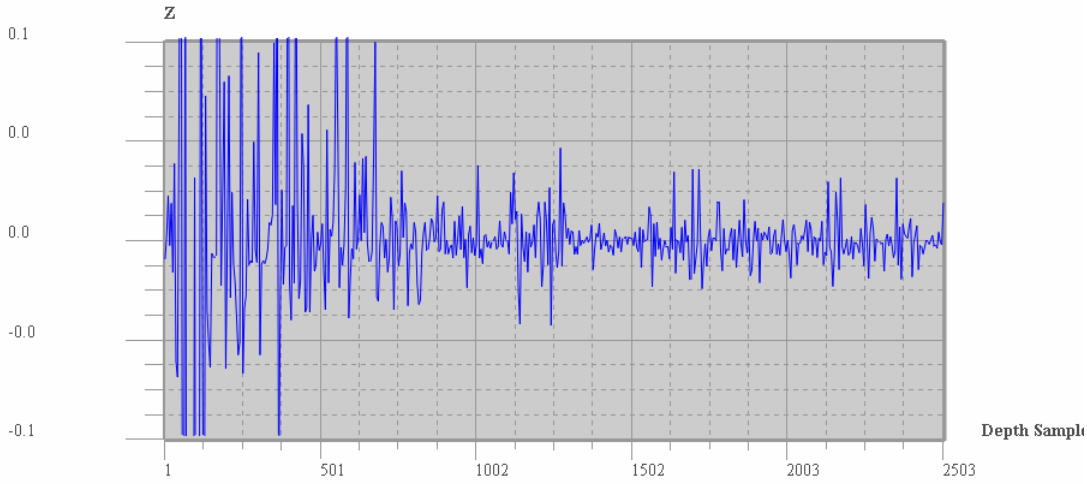

Figure 7A. Zöppritz reflection coefficients for well 5-7. The x axis is the depth sample number, corresponding to depths from 67.5 ft. to 1318.5 ft. The y axis is the real part of the full Zöppritz reflection coefficient averaged over offsets from 100ft. to 1200ft. The scales are the same as figure 6.

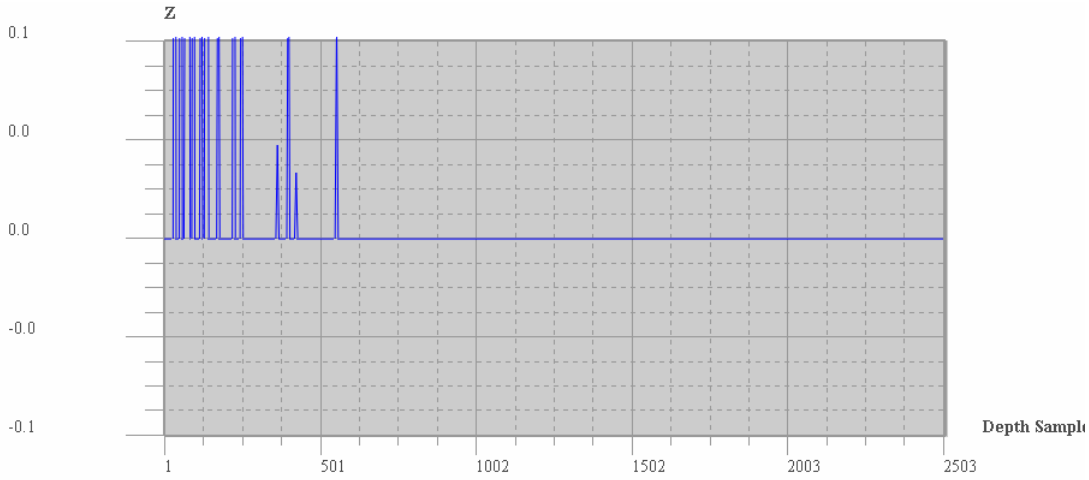

Figure 7B. Zöppritz reflection coefficients for well 5-7. The x axis is the depth sample number, corresponding to depths from 67.5 ft. to 1318.5 ft. The y axis is the imaginary part of the full Zöppritz reflection coefficient averaged over offsets from 100ft. to 1200ft. The scales are the same as figure 6.

For roughly the bottom two thirds of the curves there is a clear resemblance, but difference in detail. For the top third, the Zöppritz results are markedly larger. For about the top quarter, the imaginary part of the Zöppritz reflection coefficient has large spikes. Recall that a non zero part in the reflection coefficient indicates a post critical reflection.

Shear Velocity Estimation

In constructing the Zöppritz reflection coefficients, it was assumed that the shear velocity was known. In the log editing section it was mentioned that the shear logs were of poor quality. Instead of using them, we choose to estimate the shear velocity form other logs. Shear velocity can be estimated within a few percent from the compressional velocity. The most accurate estimates require knowledge of the lithology. Our method of obtaining the lithology is discussed in the next section. Given the lithology, we mix trend curves for pure end member lithologies to produce a mixed lithology trend, which we then use. Note that a different trend is used for each depth, since each has its own lithology.

Although not a concern for our data, in general the measured compressional velocity and density may be for a region with hydrocarbon saturation. Now the trend curves that we want to use are valid only for brine saturated rocks. The solution is to solve the Gassmann fluid substitution equation simultaneously. (Greenberg and Castagna 1992) Our implementation is in the same spirit as Greenberg and Castagna, with some modifications to insure mathematical robustness. The details are given in Appendix B.

The results of the shear velocity estimation are given in figure 8.

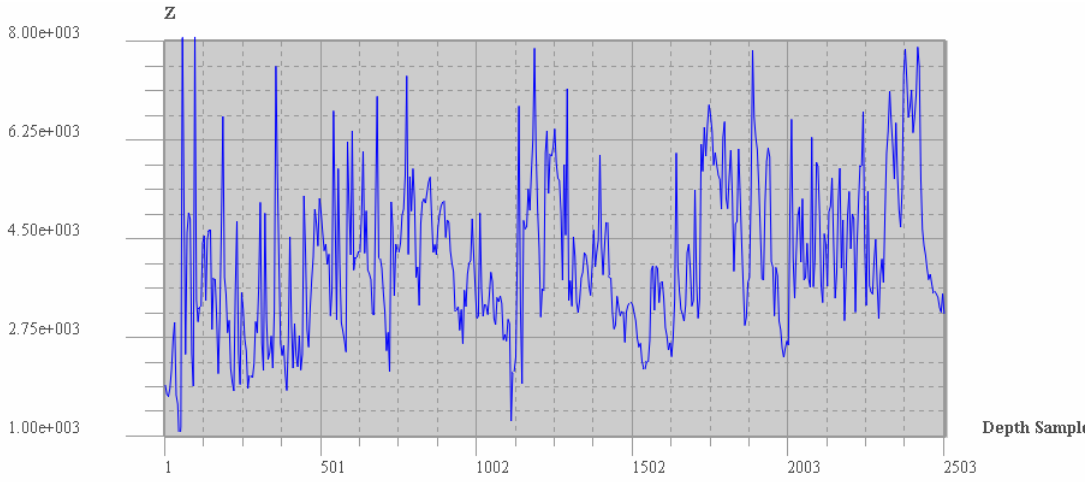

Figure 8. Estimated shear velocity. The x Axis is depth samples, corresponding to 55 ft. to 1377 ft. The y axis is shear velocity in Kft/sec.

It should be noted in passing that shear velocity estimation can be an aid to log editing, since it is rather sensitive to glitches on the logs.

Lithology Analysis

It is clear from inspecting the logs that there are a few small zones for which a sand/shale model are inadequate. Thus we choose a sand/shale/lime lithology model. The gamma ray, spontaneous potential, bulk density, photoelectric effect, neutron porosity, shallow, medium and deep resistivity, and compressional sonic logs are available at well 5-7.

The gamma ray and spontaneous potential are used only to indicate “pure” shale zones. These zones are used to estimate shale properties. Properties of other minerals can be obtained from tables. The resistivity logs are normally used to obtain hydrocarbon saturation, but we know that all zones of interest here are brine filled.

The remaining logs (bulk density, photoelectric effect, neutron porosity and sonic) are sufficient to do a 4 mineral plus porosity lithology analysis. We choose to limit ourselves to 3 minerals, and have an overdetermined problem. Then we solve using least squares. All tool equations are assumed to be linear. The results of the lithology are given in figure 9, and the porosity in figure 10.

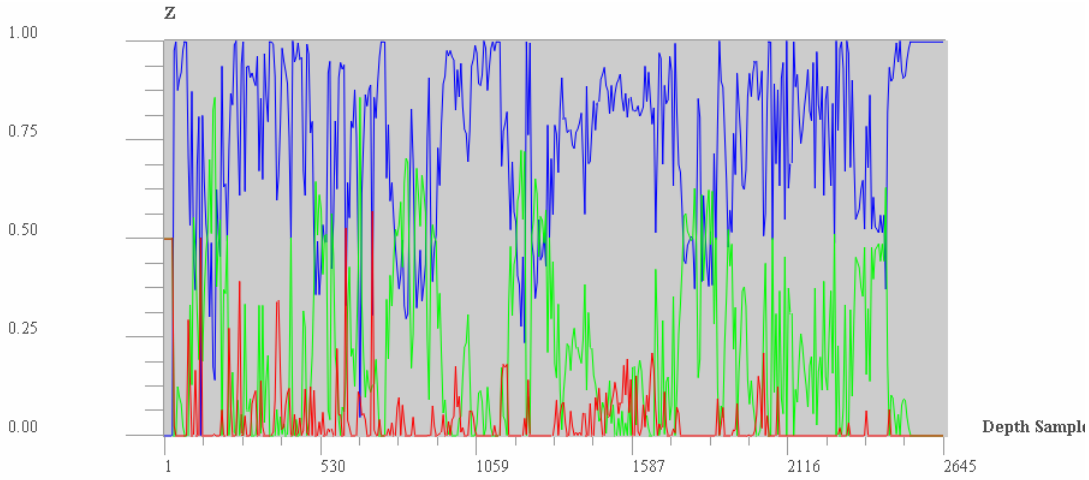

Figure 9. Lithology analysis. Blue curve is shale, Green is Sand and red is lime. The x axis is depth samples corresponding to 55ft. to 1377 ft. The y axis is volume fraction for the mineral.

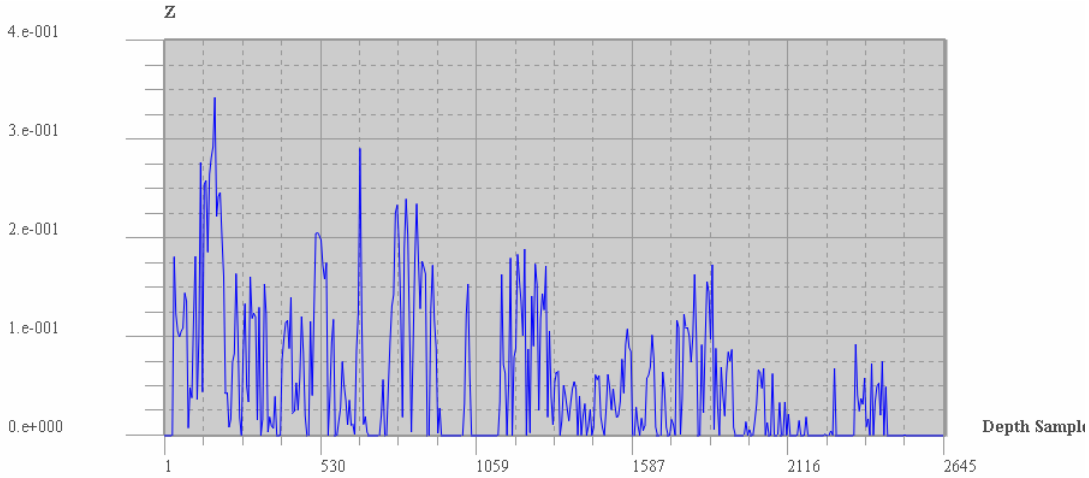

Figure 10. Porosity. The x axis is depth samples corresponding to 55ft. to 1377 ft. The y axis is porosity.

Preliminary Synthetics

Proper synthetic seismograms should be made using the correct wavelet. This is necessary to do quantitative seismology. But even without the correct wavelet, there is a lot to be learned from making preliminary synthetics. To go from the reflection coefficients in depth that were derived above to preliminary synthetics we need a time to depth curve and a preliminary wavelet.

To get the preliminary wavelet, we want to match the frequency spectrum in the real data. We average a few traces near well 5-7 which had minimal processing, and were stacked only out to 1200 ft. Then the zero phase wavelet with the same spectrum of the averaged trace is

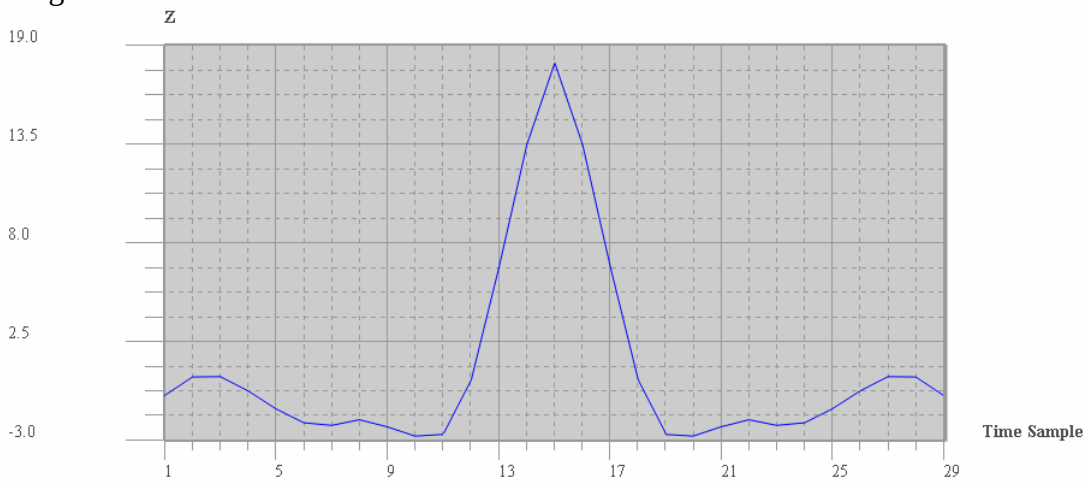

Figure 11A. Zero phase wavelet with same spectrum as average of traces near well 5-7. The x axis is time samples of 1 ms. The Y axis is amplitude.

Phase shifting this 90 degrees gives

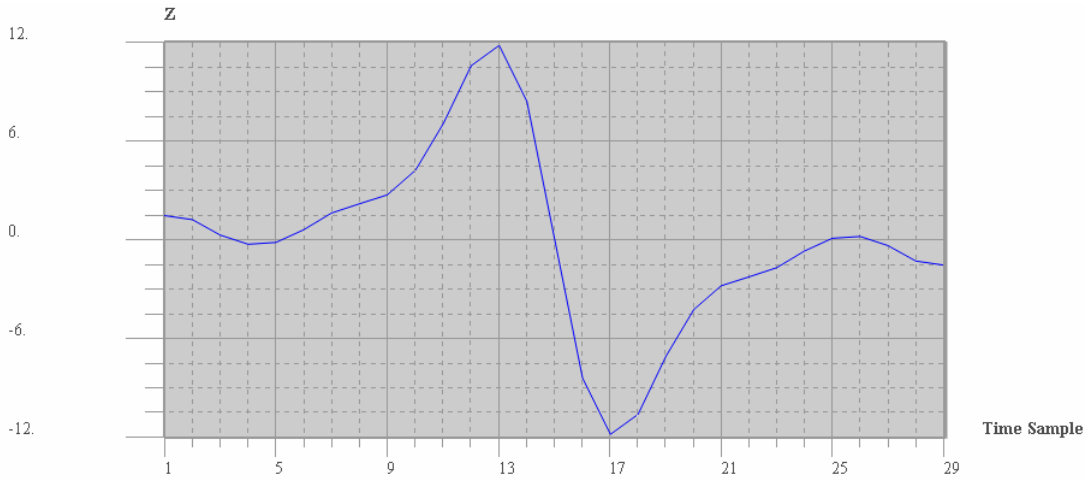

Figure 11B. 90 degree phase shift of the wavelet in figure 11A. The x axis is time samples of 1 ms. The Y axis is amplitude.

To get the time to depth curve, it is traditional to begin by summing the sonic log. This ignores short period multiple effects. To do somewhat better, a window of a time corresponding to some fraction of a wavelength at the dominant frequency of the seismic data. Then for each depth, the sonic and density logs are blocked (in depth) with blocks

of time thickness equal to the time window value. Blocking is done from the bottom up, leaving a partial block on the top. The blocks are Backus averaged (Backus 19??) and the vertical transit times summed. At least for this case, the results are nearly independent of any reasonable choice of the window length.

To get the time to depth curve aligned with the seismic, one must know a constant which gives the time on the seismic at the depth of the topmost level of the well logs. This is estimated using the datum and replacement velocity used in seismic processing, and an estimate of the average velocity above the logged interval.

With this preliminary estimate, we proposed previously to improve the T(Z) function by applying a linear stretch between events, and smoothing the corners. This presumed that characteristic events with good separation could be identified on both data and synthetic. Unfortunately, this is true in our case.

One way to get around this problem is to use the VSP at well 5-7. The drift between our preliminary estimate and the VSP values processed by Moreno are given in figure 12.

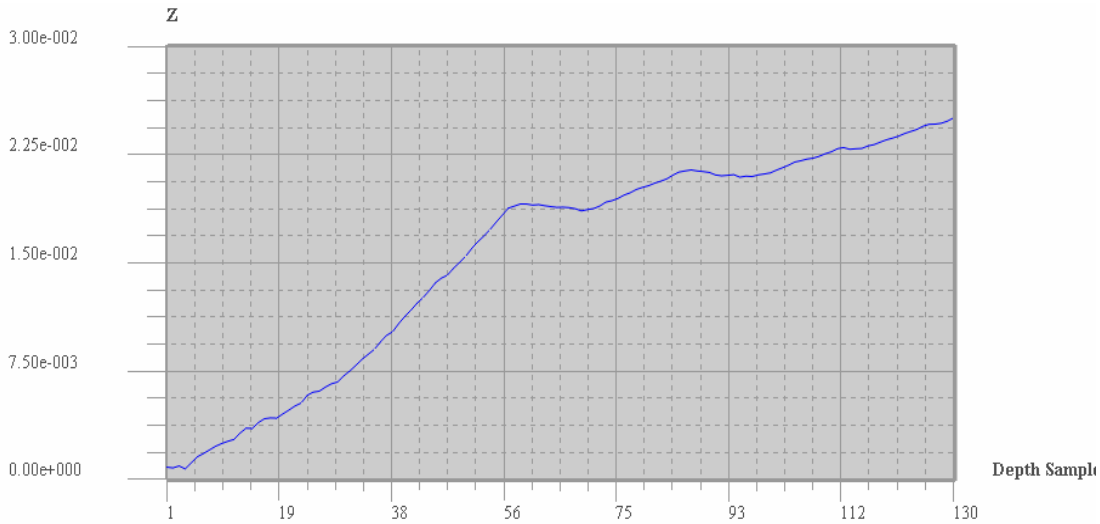

Figure 12. The difference between the VSP transit time vs depth and a preliminary estimate from well log data. The x axis is depth samples which correspond to 400 ft to 1235 ft. The y axis is the deviation in seconds.

To incorporate this drift an additive correction is introduced to the preliminary T(Z) curve. The correction is presumed to be piecewise linear (with some rounding at transitions between slopes). Then a least squares fit is done to the drift curve. The slopes can be determined using linear algebra, but the transition depths affect the result non linearly. They are determined by a brute force parameter search. Figure 10 gives the fit that was obtained.

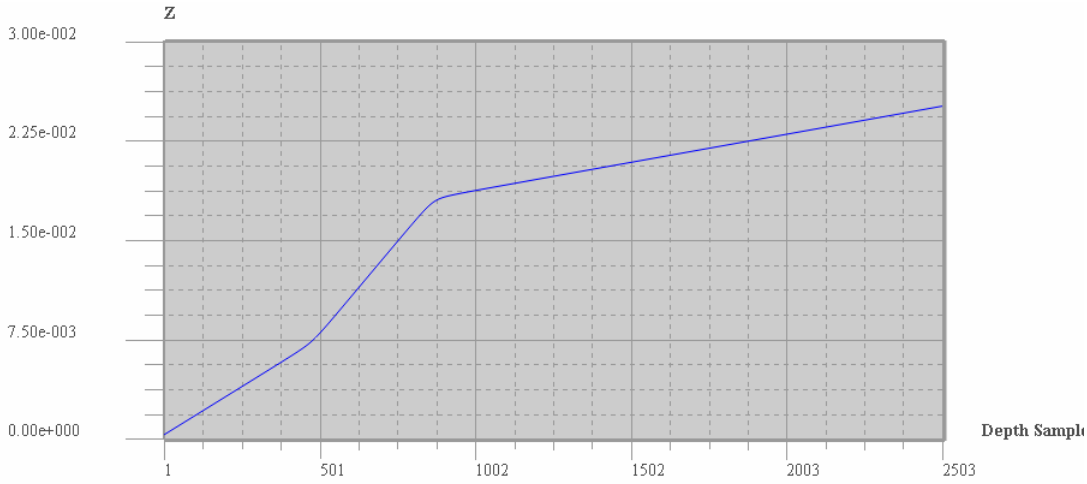

Figure 13. Time to depth curve additive correction. Least squares fit to the data in figure 10. X axis is depth samples corresponding to 67.5 ft. to 1318.5 ft.. Y axis is the deviation time in seconds.

Now preliminary synthetics can be made. Using normal incidence reflection coefficients and the zero phase preliminary wavelet of figure 11A give the synthetic in figure 14A. Figure 14B is the same except the 90 phase shifted wavelet of figure 8B is used.

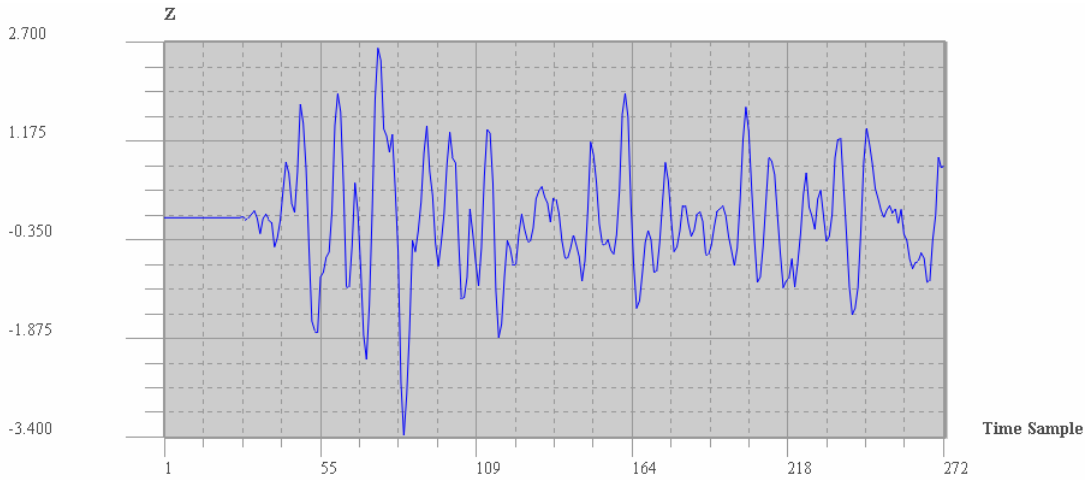

Figure 14A. Synthetic seismogram using normal incidence reflection coefficients and zero phase preliminary wavelet from figure 11A. The x axis is time samples of 1 ms. The Y axis is amplitude.

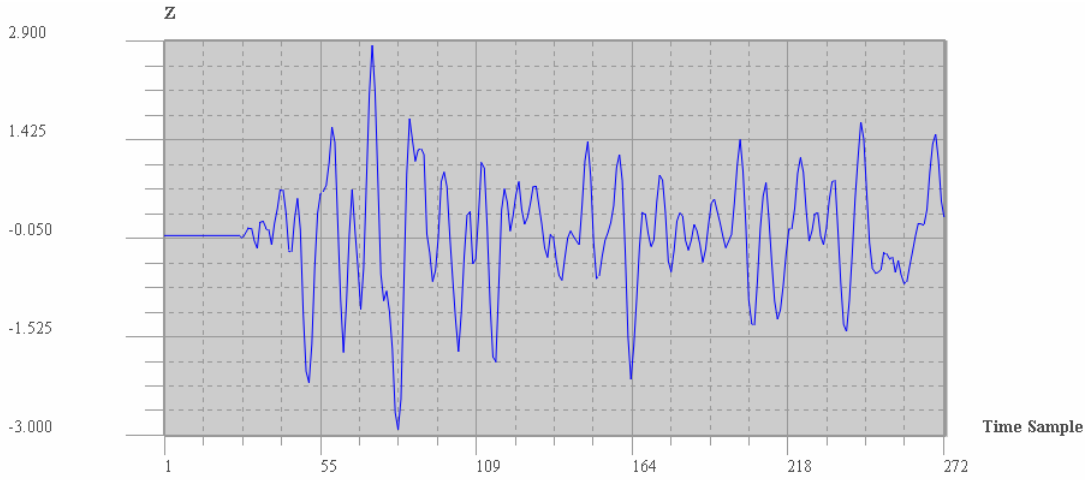

Figure 14B. Synthetic seismogram using normal incidence reflection coefficients and 90 degree phase shifted preliminary wavelet from figure 11B. The x axis is time samples of 1 ms. The Y axis is amplitude.

Using the real part of the Zöppritz reflection coefficients gives figure14A for the zero phase wavelet and figure 14B for the 90 degree phase shifted wavelet.

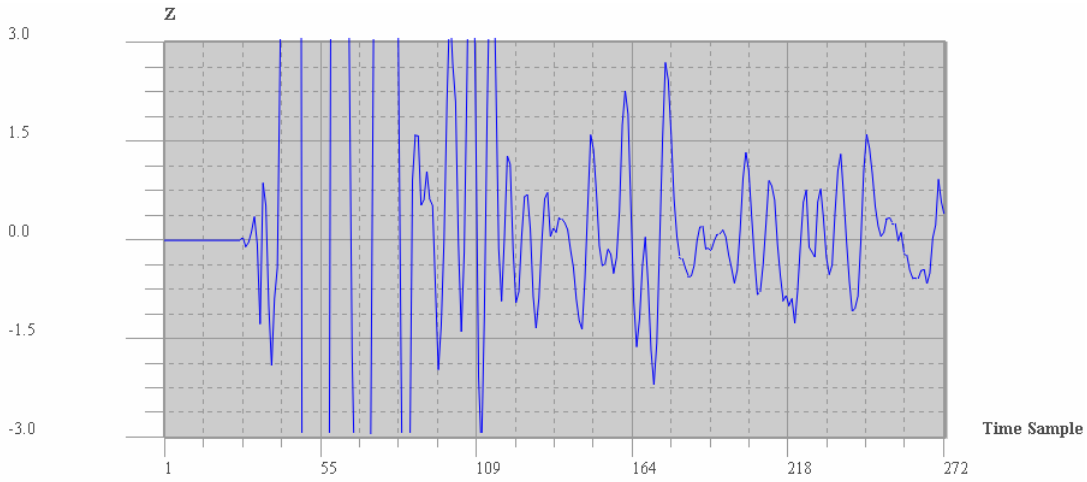

Figure 15A. Synthetic seismogram using real part of Zöppritz reflection coefficients and zero phase preliminary wavelet from figure 11A. The x axis is time samples of 1 ms. The Y axis is amplitude.

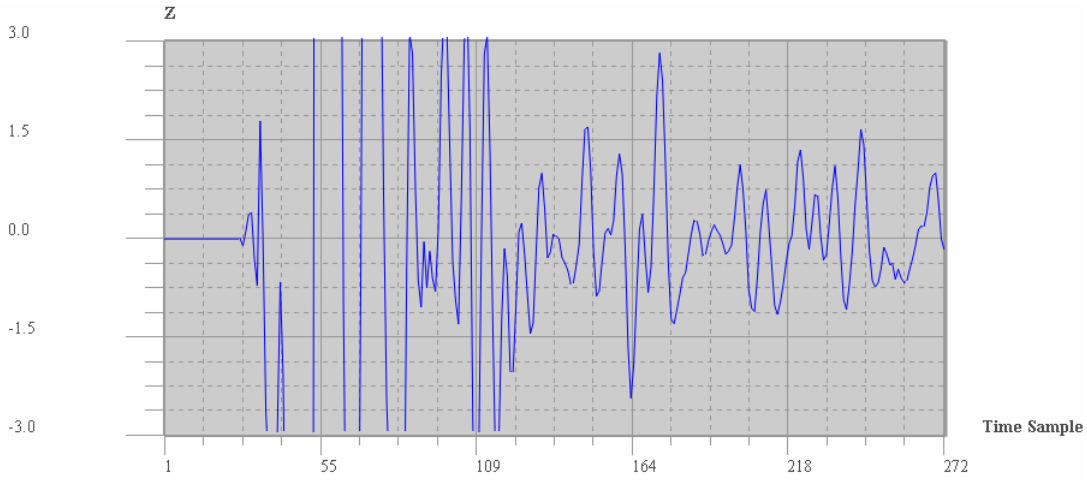

Figure 15B. Synthetic seismogram using real part of Zöppritz reflection coefficients and zero phase preliminary wavelet from figure 11B. The x axis is time samples of 1 ms. The Y axis is amplitude.

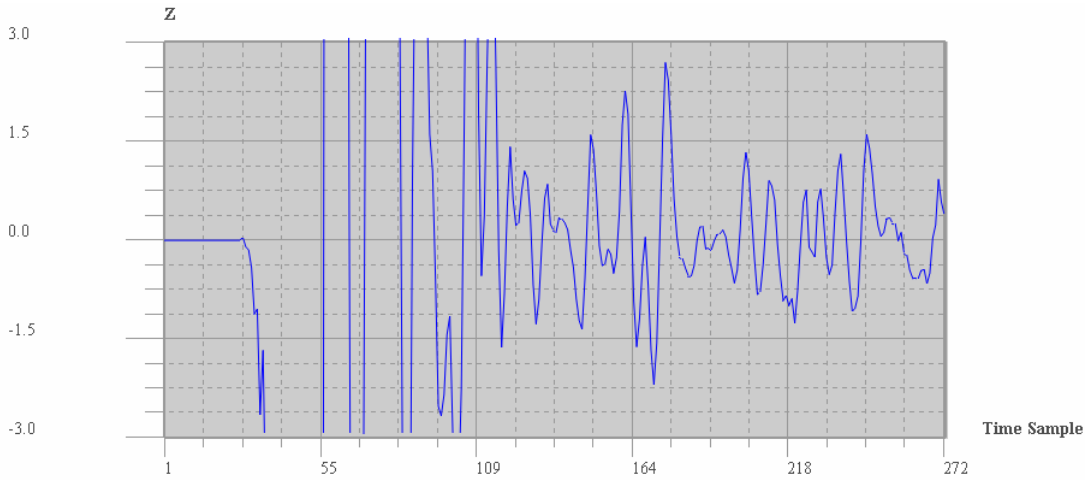

Figure 16. Synthetic seismogram using complex Zöppritz reflection coefficients and zero phase preliminary wavelet from figure 11A. The x axis is time samples of 1 ms. The Y axis is amplitude.

The results for the synthetic seismograms (not surprisingly) parallel those for the reflection coefficients. At the top of the interval, the amplitudes of the events are very large when using angle dependent reflectivities. In the top quarter, with many post

critical reflections, proper convolutional synthetics should use the complex reflection coefficients (Figure 16). The differences with using the real part of the reflection coefficients only is shown in figure 15a. The differences are substantial but are obscured by the clipping. Comparing the normal incidence results (figure 14) and the angle dependent results (Figure 15), we find they become more alike in amplitude and shape as we go deeper in the interval, but noticeable differences remain.

The one firm conclusion that can be made is the angle dependence of the reflectivity is important, even in the deeper part of the interval where the Gypsy interval occurs.

Seismic Data

Good processing of the seismic data is essential to quantitative seismology. One needs to understand exactly what processes have been applied to the data, and to tailor these to match the intended use of the data. With this in mind, and to take advantage of the improvement of seismic processing software in the last decade, Carlos Moreno has undertaken to reprocess the data. A decade ago only large oil companies or seismic contractors could undertake to process a 3D data set. Today it is possible for this to be done even with university facilities.

The shallow region of interest presents special problems. Surface waves and refracted arrivals are especially strong in this region. One typical method of dealing with this problem is to mute the regions containing offending events. At depth, this is not a big problem, but for shallow zones, much of the data is muted as well.

Dealing with shallow data is difficult for another reason: most processing software development was done with a view to enhance deep targets. Special problems with shallow data have been ignored as of little economic interest.

Reprocessing is now underway. Multiple versions of processed data have been produced, although more remains to be done. Even at this stage several things are clear. First, the amplitude of the very early events is quite large, qualitatively in agreement with the results of the Zöppritz modeling, but not in agreement with the normal incidence modeling. Second, the quality of the results is even more sensitive to the choice of processing parameters and processes than is usually the case. Third, considered as an attempt to work with targets at depths of a few thousand feet, this is an excellent quality data set.

Above, we noted the importance of the angle dependence of the reflection coefficients. This can be addressed by including it in the modeling of the synthetic seismograms, or by muting the large angle zones in processing. It is not clear a priori which is better. Carlos Moreno is experimenting to help decide this issue.

Finally, variations in fold and offset/azimuth coverage will make quantitative comparisons of events across the range of the survey especially difficult. Nevertheless, we proceed to attempt just that in the next section,

Part II: Optimal Attributes

A seismic event is represented as a time series of amplitudes. Usually one does not attempt to use each amplitude sample as an independent piece of information to be related to the geology that one is trying to characterize. Rather, one works with some smaller set of numbers derived from the original time series, which purport to contain the information needed for our interpretation. These are called attributes. There are an infinite number of ways to define attributes. Peak or trough amplitude, peak width, intervals between peaks or zero crossings and numerous combinations of the preceding just begin to sample some of the attributes that people have used. Another set of attributes: frequency, phase and envelope amplitude for a given time are common. In sum contexts attributes means these attributes. That is not what we mean here.

There are two qualities that one would like in attributes: data reduction and interpretability. The first just means the effectiveness of reducing the N numbers of the time series to M attributes, with M smaller than N, without losing interpretationally useful information. The second means that one can directly interpret an attribute as a geologically significant parameter. For example, under certain circumstances, the time separation of a peak and trough is a scaled measure of formation thickness.

Unfortunately, both of these criteria seldom go together. Here we will obtain attributes that are optimal in the data reduction sense, and only later attempt to relate them to quantities of interpretational interest. To be precise, consider a portion of a seismic section containing an event S_i^k, where k indexes the trace and i indexes the time samples. The event is then represented in the form

$$S_i^k = \sum_{j=1}^{N} a_j^k v_{j,i} \qquad (5a)$$

where N is the number of terms in the time series. The $\{v_{j,i}\}$ can be grouped into N time series $\{\mathbf{v_j}\}$. They are assumed linearly independent, but with no further restriction at this point. The $\{a_j^k\}$ are the attributes, where j indexes attribute number and k indexes the trace. Attributes can always be found to satisfy equation 5a.

The $\{\mathbf{v_j}\}$ are at our disposal. To define them to provide maximum data reduction, we consider the truncated sum

$$S_i^{k(M)} = \sum_{j=1}^{M} a_j^k v_{j,i} \qquad (5a)$$

where $M < N$. The criteria for determining the $\{\mathbf{v_i}\}$ is to minimize

$$O(M,\{\mathbf{v_i}\}) = \sum_{i,k} (S_i^k - S_i^{k(M)})^2 \qquad (6)$$

To achieve this we perform a singular value decomposition of S (Press et. al. 1992)

$$S_i^k = \sum_{j=1}^{N} u_{k,j}\, e_j\, v_{j,i} \qquad (7)$$

where the matrices are orthogonal: $u^T u = v^T v = 1$. Without loss of generality, we can take the e_i to decreasing in absolute value. The attributes can be identified as

$$a_j^k = u_{k,j}\, e_j \qquad (8)$$

Using the orthogonality properties of u and v, it can be shown that

$$O(M) = \sum_{j=1}^{N-M} e_j^2 \qquad (9)$$

or, alternatively, the contribution to the energy of the event from each component $\mathbf{v_j}$ is e_j^2. Now, we must show that the choice of V from the singular value decomposition is in fact optimal. Assume an alternative decomposition to equation 7:

$$S'^k_i = \sum_{j=1}^{N} b_{k,j}\, w_{j,i} \qquad (7)$$

where w is another orthonormal basis. Then there is an orthogonal matrix Q such that

$w = Q\, v$. After a little algebra, we find the contribution to the energy of the M term truncation of this expansion is

$$E'(M) = \sum_{l=1}^{M} \sum_{j=1}^{N} Q_{l,j}\, e_j^2 \qquad (8)$$

since Q is an orthogonal matrix

$$E'(M) < \sum_{l=1}^{M} e_j^2 \qquad (8)$$

so that M terms in the alternate expansion contains less energy in the SVD expansion.

One very important fact can be immediately determined upon the definition of the SVD optimal attributes. Only waveforms **v** which contribute significantly to the energy of the event can be useful for robust estimation. This means that if only M waveforms are significant, no more than M parameters can be robustly estimated simultaneously. This provides a considerable knowledge about how much to expect from an interpretation.

To this point, a set of attributes has been derived that is maximally effective in accounting for our event, but to this point has no connection with subsurface geology. To make this connection, geological models will be constructed and synthetic seismograms generated. These synthetic seismograms will be processed to obtain attributes by expanding in the basis functions that were found optimal for the seismic data. The synthetic seismograms provide a calibration of the attributes. As an example of this process, consider the calibration plot in figure 17.

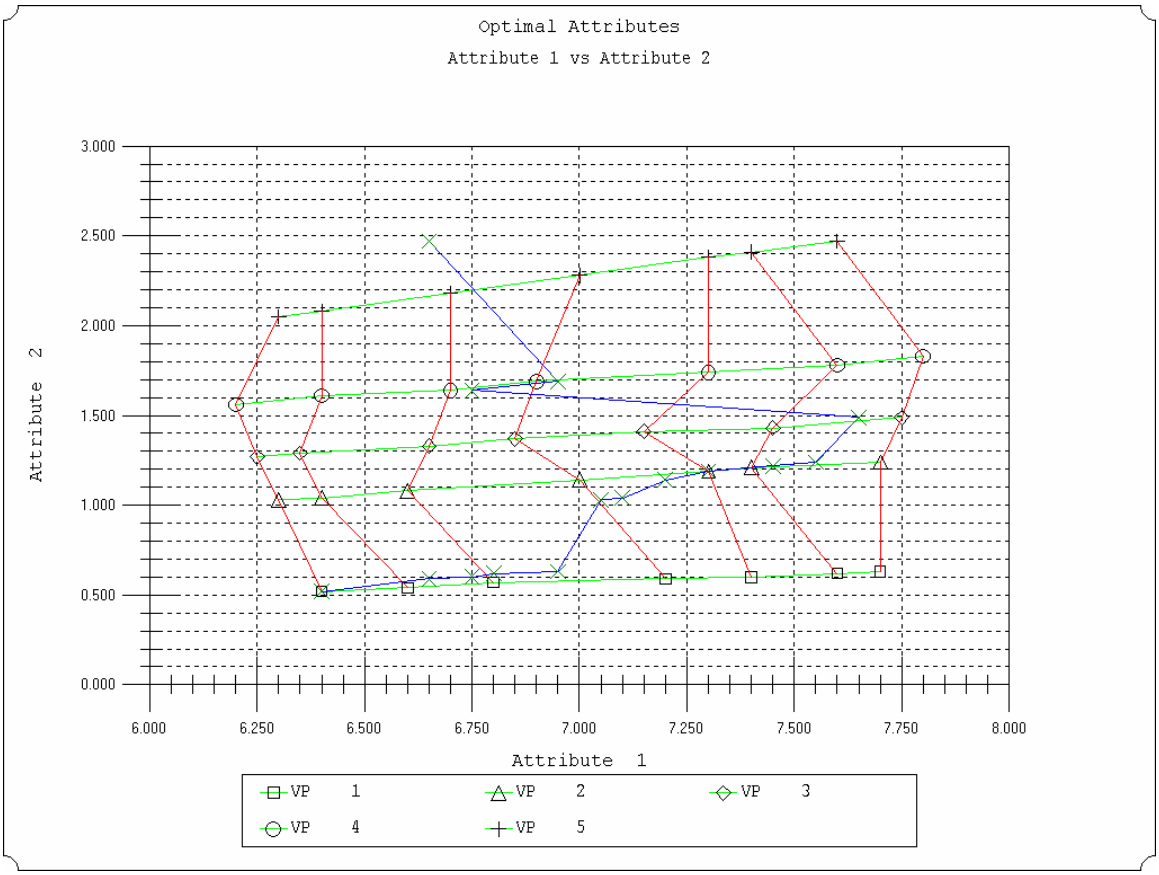

Figure 17. An example attribute calibration plot. (Not the result of real data)

The axes have been chosen as the first two attributes. Each synthetic seismogram is represented as a point in N dimensional space, whose coordinates are the values of its N attributes. The plot shows the two dimensional projection of the N dimensional points representing the synthetic seismograms., in this case axes 1 and 2. The green lines connect points on the plot associated with synthetic seismograms having some parameter of the geological model fixed, in this case the compressional velocity. Another set of (red) lines will connect points with another parameter fixed, e.g. the thickness of a layer. For two sets of lines (and parameters) we get a distorted grid. Each set of lines indicates a contour of its associated parameter.

The real data are shown as blue X's connected by a blue line. For a moment let us consider only two attributes and two geological parameters. Pick a real data point. If it is

in a distorted box defined by two contour lines for each parameter. The interpretation given to the seismic point is that it results from geology described by parameters somewhere in the box. If not, like the last real data point on the example plot, the underlying geology is presumed not to lie in the range of geological models used to generate the calibration synthetics.
The calibration plot also acts a form of sensitivity analysis. When contour lines are well separated, that parameter can be robustly estimated, when this is not the case, robust estimation is not possible.

Finally, we can do inversion. Using the synthetics as calibration, we can tile a region of N space with closed polygons whose vertices correspond to synthetics made using certain geological parameters. Then each seismic trace will produce a point in N space. If it is inside one of the polygons defined by the synthetics, we interpolate the geological parameters that belong to each vertex to provide the geological parameters for the real data trace.

A flow chart of the entire process is shown in Figure 18.

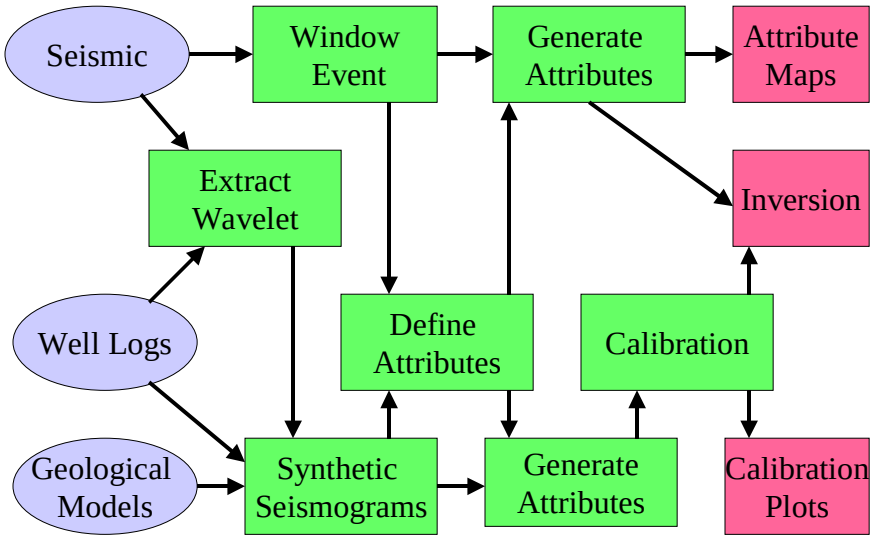

Optimal Attribute Flow Chart

Figure 18. Flow Chart for Optimal Attribute Procedure

A First Look at Gypsy Data

For our first look at using optimal attributes on the gypsy data, we choose to work with the strongest event in our data set above .3 seconds. This data set was processed using heavy muting, and smoothed laterally using FX decononvolution. The event is centered at

~.22 sec near the geographic center of the seismic survey. It corresponds to a depth of about 835 ft. It does not correlate with any of the major sand packages. There is gentle dip to this event as can be seen in Figure 19.

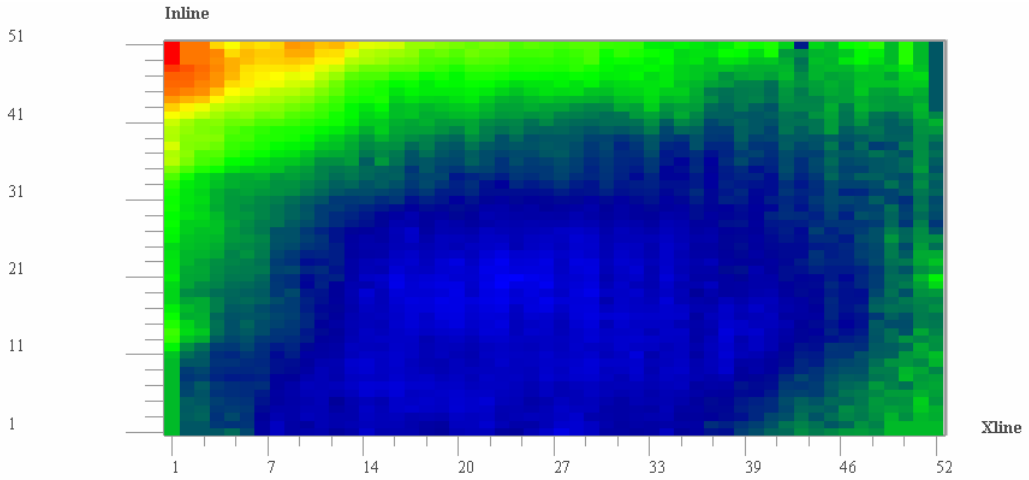

Figure 19. Time pick for minimum of waveform in event selection window. Difference between red and blue is 10ms.

After finding the center of the event, a window of 25 ms, about the picked centered event is used as input to the optimal attribute procedure. The results in figure 20 show that about 70% of the data can be explained by reconstructing with only 3 eigenvectors.

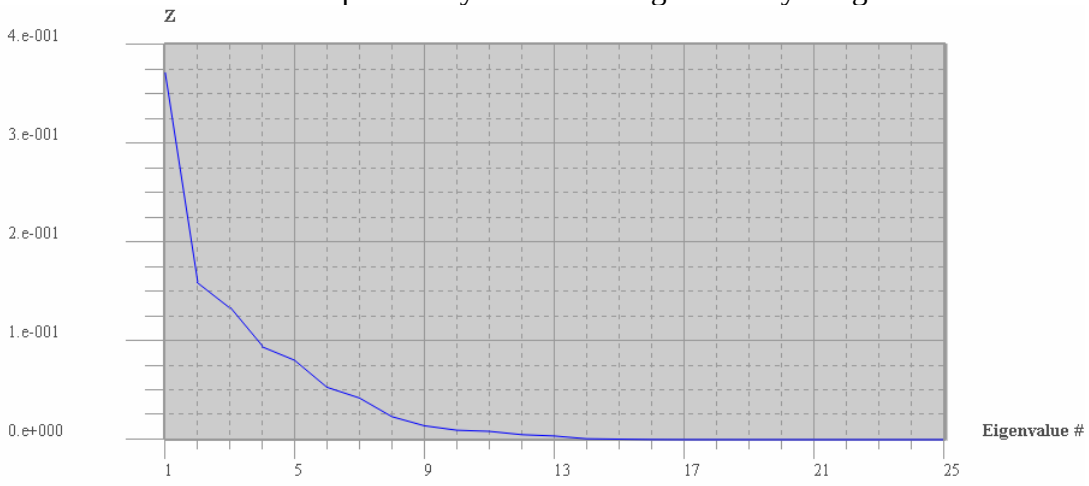

Figure 20. Normalize squares of eigenvalues from optimal attribute definition.

The waveforms for these first three eigenvectors are given in figure 21. For comparison, the average waveform for the window is shown in figure 22. It is apparent that the first eigenvalue (blue) shows considerable resemblance to the average waveform, but that they are not identical.

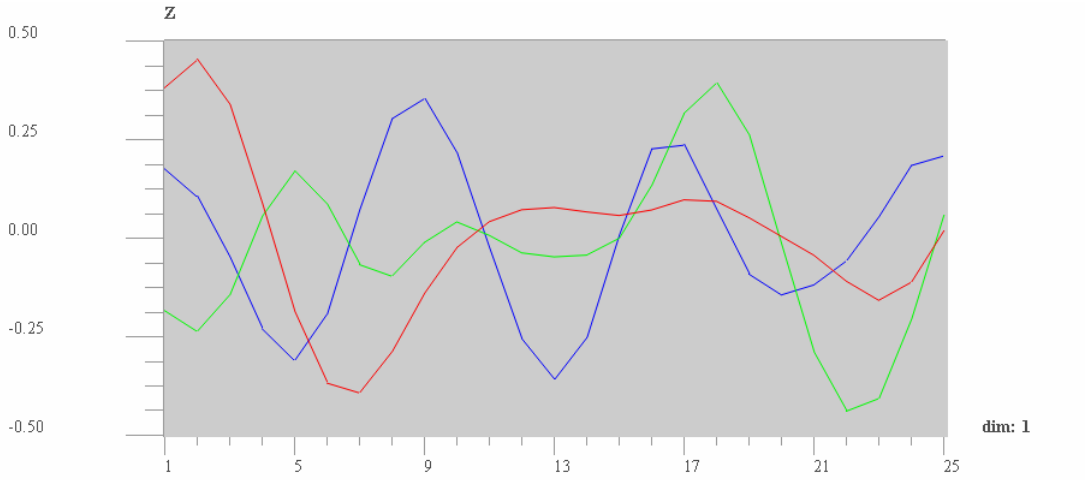

Figure 21. Waveforms associated with first three eigenvalues. X axis is time samples in ms., and Y axis is amplitude. The order of the curves is blue, green, red.

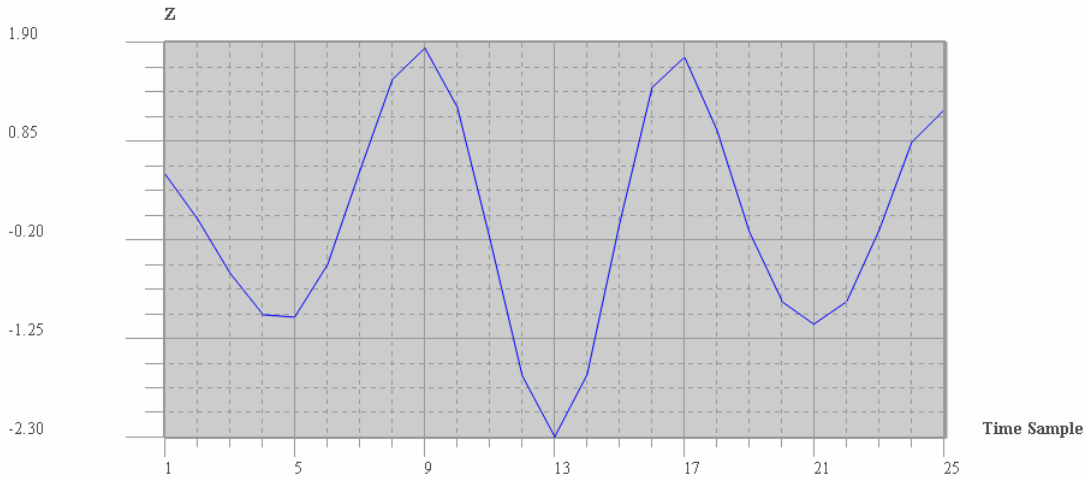

Figure 22. Average waveform in window.

We now look at maps of the first three attributes, given in figures 23a, 23b and 23c. All three shown systematic variation, but the regions of variation appear to be different.

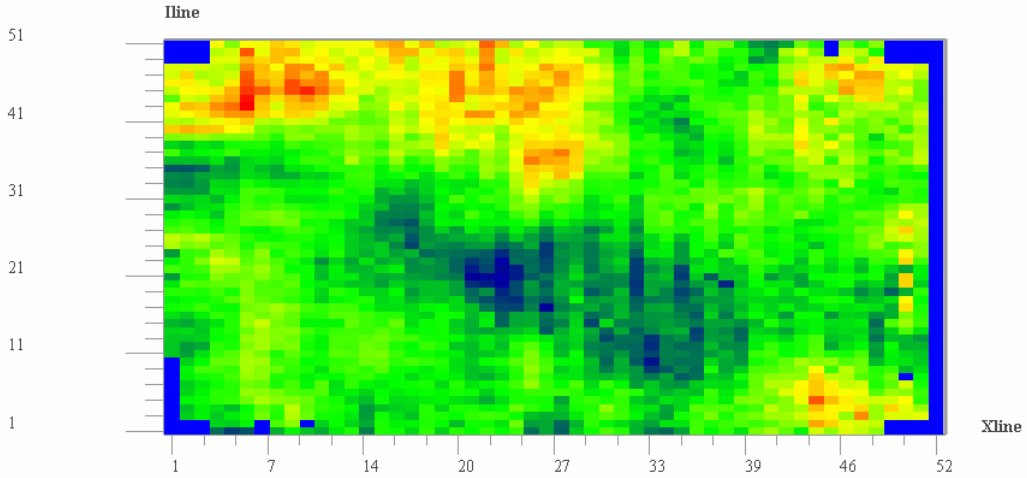

Figure 23a. Map of first optimal attribute.

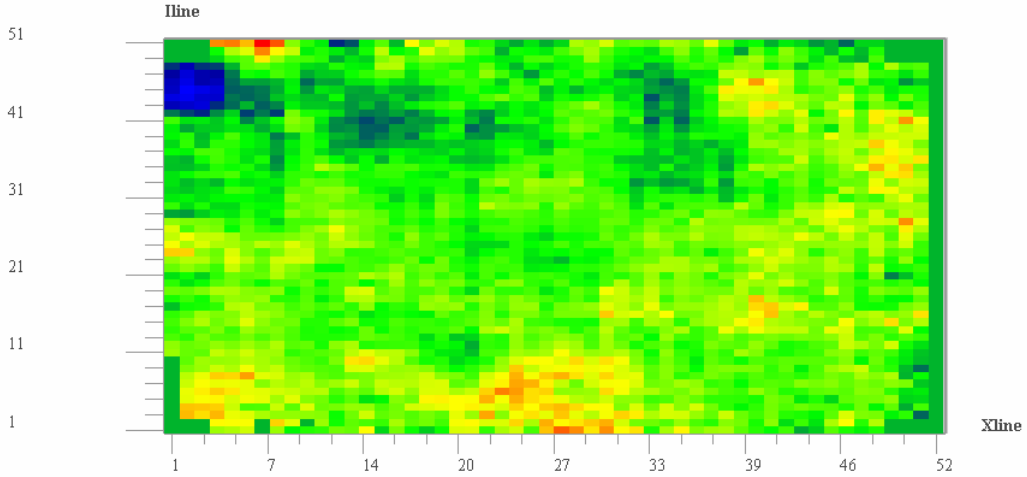

Figure 23b. Map of second optimal attribute.

Interpretation of these maps will be deferred until the attributes have been calibrated. At this point, about all one can say is that Figure 23a is probably not very different from a trough amplitude map for the same event, because of the similarity of the first eigenvector and the average waveform. It is unclear at this point if we are really looking at something geological, an acquisition footprint, or a processing artifact.

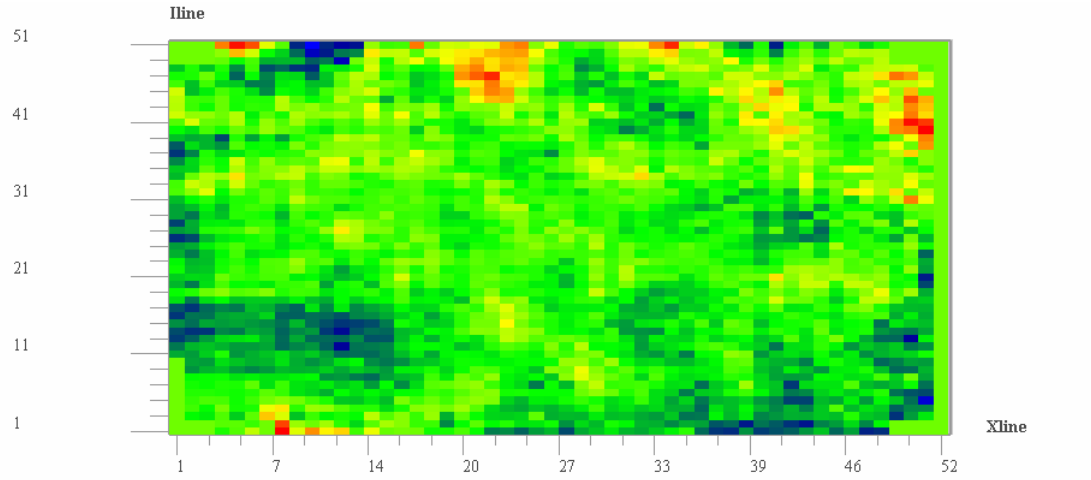

Figure 23c. Map of third optimal Attribute.

Status and Plans

Since the last report it been determined that the bad match between synthetics an real data is a result of all three of the possible causes: bad log data, bad seismic data and inadequate software.

The well logs were found to have many problem areas, especially the full waveform sonic logs. Well log problem has been addressed and logs edited. Adequate log data is now available, except possibly in the very shallow part of the section.

With regard to software, it has been demonstrated that offset dependence in reflectivity cannot be ignored. Software addressing this problem within the convolutional model framework has been written. For the earliest ~.1 second of data it is unlikely that a convolutional approach can be successful, as it does not account for transmission losses and non plane incidence.

Carlos Moreno has produced a series of reprocessings of the seismic data. He has shown conclusively that the result is very sensitive to the choice of processing parameters. We still do not have any seismic data that tie well with our synthetics, but the agreement in much better previously obtained.

Since we still cannot get adequate ties, a good wavelet extraction and subsequent quantitative seismology is in the future.

Nonetheless, we have proceeded to work on a scheme using optimal attributes to provide a detailed, quantitative, small scale interpretation. For a particular event, we have quantified the importance of various attributes and produced maps of optimal attributes. Lack of a good tie has so far precluded calibration using of the attributes using synthetics. In fact, at this early stage it is not clear that the attribute variations are due to geology and not acquisition and processing.

The first order of business for the future is to continue the work to get a good tie. Processing will likely be the key. Then an attempt can be made to extract attenuation information. Again, after we get a good tie, we can use the optimal attribute approach to help understand just how much data there is in the seismic, and what it can tell us about reservoir properties.

References

Backus, George, Long-Wave Elastic Anisotropy Produced by Horizontal Layering, Journal of Geophysical Research, Vol. 67, No. 11, October 1962, pp. 4427-4440

Berryman, James, Long-wavelength Propagation in Composite Elastic Media I. Spherical Inclusions, J. Acoust. Soc. Am. 68(6), Dec 1980, pp.1809-1819

Brown, R.J.S. and Korringa, J.; On the Dependence of the Elastic Properties of a Porous Rock on the Compressibility of Pore Fluid, Geophysics, Vol. 40, No. 4, (August 1975), P. 608-616

Castagna, J.P., Batzle, M.L. and Kan,T.K. Rock Physics – The Link Between Rock Properties and AVO Response, pp 135-171 in Castaga, J.P. and Backus, M.M., Offset-Dependent Reflectivity – Theory and Practice of AVO Analysis, SEG, Tulsa, 1993

Gassmann, F., 1951, Über die Elastizität poröser Medien; Vierteljahrschrift der Naturforschenden Gesellschaft in Zürich, v.96, p. 1

Greenberg, M.L. and Castagna, J.P., Shear-wave Velocity Estimation in Porous Rocks: Theoretical Formulation, Preliminary Verifications and Applications, Geophysical Prospecting 40, PP 195-209,1992

Lamb, William, Progress Report: Absorption and Dispersion from Gypsy Data, DOE Gypsy Field Project Report, 1998

Moreno, Carlos, 2000, Elsewhere, this report.

O'Douhery, R.F. and Antsey, Nigel, 1971, Reflections on amplitudes: Geophysical Prospecting 19, pp 430-458

Press, W.H., Teukolsky, S.A., Vettering, W.T. and Flannery, B.P., 1992, Numreical Recipes in Fortran, the Art of Scientific Computing,Cambridge University Press

Seifert, Dirk, 1994, Reservoir Development Scale Modeling Based on Integration of High Resolution 3-D seismic Data, well-logs and core Data: Gypsy site, Pawnee County, Oklahoma, USA, Masters Thesis, University of Oklahoma

Thomsen, Leon, Weak Elastic Anisotropy, Geophysics, 51, 1986, p. 1954-1966

Young, G,B, and Braile, L.W., A Computer Program for the Application of Zoeppritz's Amplitude and Knott's Energy Equations, Bulletin of the Seismological Society of America, Vol. 66, No. 6, pp. 1881-1885, December 1976

Zheng, Xiaodong, Approximations to P-P,P-SV, SV-SV and SV-P Reflections and Transmissions, SEG Expanded Abstract SL3.8, 1991, pp. 1102-1105

Appendix A

Ray Tracing in Layered Media

To use angle dependent reflection coefficients, the incidence angles must be computed. The simplest way to accomplish this is to trace rays through layered media. This procedure assumes a plane wave source, and considers only the true primary reflection (i.e. multiples are ignored.) We have the situation in figure A1.

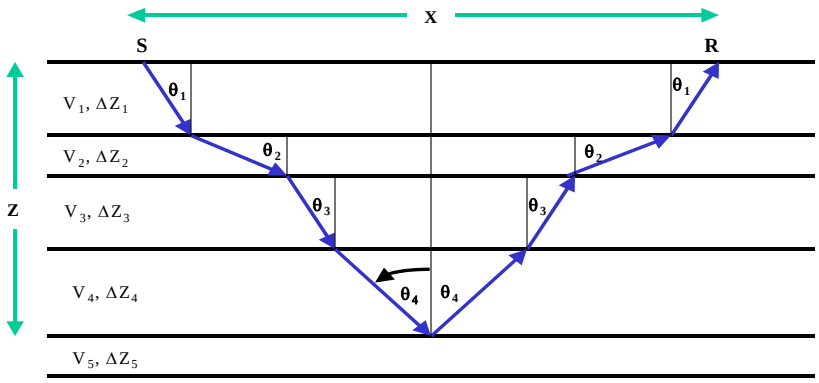

Figure A1. A ray begins at source S, travels through layers 1 through 4, reflects at the interface between layers 4 and 5, then travels through layers 4 through 1 to receiver R. Layers have velocity V and thickness Δz.

The offset X and the depth Z are given, but the angles must be determined. Now, Snell's law can be written

$$p = \sin(\theta_1)/V_1 = \sin(\theta_2)/V_2 = \ldots = \sin(\theta_n)/V_n \qquad \text{(A1)}$$

where p is called the ray parameter. The offset can be obtained from

$$X = \Sigma\, \Delta X_i = \Sigma\, \Delta Z_i \tan(\theta_i) \qquad \text{(A2)}$$

Using equation A1, this can be written

$$X(p) = \Sigma \{ (\Delta Z_i \, p \, V_i) / (1 - (p \, V_i)^{1/2})\} \quad \text{(A3)}$$

So that X is now a function of p. Ray tracing thus consists in finding the p for which the computed and given X agree. Finally, from p, the incidence for reflection θ_n can be obtained from equation A1.

Unfortunately for this naïve approach, it is well known the short period multiples do have a dominant impact on waves traveling through a stack of many layers. The effect is to reduce the amplitude of the true primary to insignificance, while producing a primary like event at a somewhat later time. Numerical solution of the wave equation will, of course, exactly take care of this issue. We would prefer something simpler, even if somewhat approximate.

The approximation process begins by noting that for long wavelengths (low frequencies) a stack of layers may be exactly replaced by its Backus average. All wave propagation effects are included. Of course, we cannot usually replace all the layers with a single Backus averaged layer because then we would not be in the long wavelength limit. We compromise by blocking the layers. In a procedure exactly analogous to that used to estimate the time to depth curve, we pick blocks of fixed length in time, The time corresponds to some fraction of a wavelength at the dominant frequency. Again, we block for each depth, working from the bottom, leaving a partial block at the top.

Except for one point, this would reduce to the original problem but with fewer layers: the Backus averaged layers are transversely anisotropic, even though the input layers are isotropic.

To accommodate transverse anisotropy, two changes must be made. Snell's law becomes

$$p = \sin(\theta) / V(\theta) \quad \text{(A4)}$$

which differs from equation a1 because the velocity depends on the angle. To be precise it depends on the phase angle θ. This is the angle related to the wavevector of the plane wave. But there is another important angle: the group angle. It is related to the perpendicular to the wavefront. Since energy moves with the group velocity, equation A2 becomes

$$X = \Sigma \, \Delta X_i = \Sigma \, \Delta Z_i \tan(\phi_i) \quad \text{(A5)}$$

where ϕ is the group angle. Thomsen (1986) gives the tangent of the group angle in terms of the velocity

$$\tan(\phi) = \{\tan(\theta) + (dV(\theta)/d\theta) / V(\theta)\} / \{1 - \tan(\theta) \, (dV(\theta)/d\theta) / V(\theta)\} \quad \text{(A6)}$$

There are three possible velocities, depending on the wave type. For SH shear waves

$$V(\theta) = \beta_0^2 \{1+ 2 \gamma \sin(\theta)\} \quad \text{(A7)}$$

where β_0 is the vertical shear velocity and γ is an anisotropy parameter.

There are two more modes, which are coupled compressional and shear waves. For quasi P- waves

$$V(\theta) = \alpha_0^2 \{1 + \varepsilon \sin^2(\theta) + D(\theta)\} \quad \text{(A8a)}$$

while for quasi SV-waves

$$V(\theta) = \beta_0^2 \{1 + (\alpha_0/\beta_0)^2 \varepsilon \sin^2(\theta) – (\alpha_0/\beta_0)^2 D(\theta)\} \quad \text{(A8b)}$$

where

$$D(\theta) = (1/2) (1 - (\beta_0/\alpha_0)^2) \{[1 + (4 \alpha_0^2 (2\delta - \varepsilon) / (\alpha_0^2 - \beta_0^2)) \sin^2(\theta)\cos^2(\theta) + (4 \alpha_0^2 \varepsilon (\alpha_0^2 (1 + \varepsilon) – \beta_0^2) / (\alpha_0^2 - \beta_0^2)^2) \sin^4(\theta)]^{1/2} –1 \} \quad \text{(A8c)}$$

and α_0 is the vertical P velocity and δ and ε are anisotropy parameters.

Using equations A5, A6 and A8, we can find X as a function of θ. Then equation A4 can be used to eliminate θ to obtain X as a function of p. This is the analog of equation A3, but here the form is more complicated. The simplest case is SH-waves

$$X(p) = \Sigma \{(\beta_{0i} p (1 - 2\gamma_i)) / [1 – \beta_0^2 p^2 (1 + 2\gamma_i)]^{1/2}\} \quad \text{(A9)}$$

This needs to be solved numerically for p, just as with equation A3. Finally, we need the phase incidence angle at the reflector

$$\sin(\theta_n) = (\beta_{0n} p) /(1 –2 \beta_{0n}^2 p^2 \gamma_n)^{1/2} \quad \text{(A10)}$$

The phase angle is required because the Zoeppritz equations expect the angle associated with the incoming plane wave, not the wavefront. For the quasi P-wave and quasi SV-wave the analogues of equation A9 can be derived analytically, but are extremely complicated. For simplicity, we consider cases where the slowness surfaces are nearly elliptical. This occurs when $\delta \sim \varepsilon$. To first order

$$X(p) = \Sigma \{ (\alpha_{0i}^2 p^2 (1 + 2 \varepsilon_i)) / (1- \alpha_{0i}^2 p^2 (1 + 2\varepsilon_i))^{1/2} + \Delta_i (Q_i^4 \zeta_i + 3 Q_i^2 –2) / ((1+2\varepsilon_i) (Q_i^2 \zeta_i+1)^2)\} \quad \text{(A11)}$$

where $R_i = \beta_{0i}^2/\alpha_{0i}^2$,$\Delta_i = \varepsilon_i - \delta_I$, $\zeta_i = 2\ \varepsilon\ R_i/\{(1-R_i)(1+2\varepsilon_i)\}$, and $Q_i = \alpha_{0i}\ p\ (1+2\varepsilon_i)^{1/2}$.

The exact expression for the phase incidence angle at the reflector is

$$\sin(\theta_n) = \{(\alpha_{0n}^2\ p^2\ W) / (1-2\ \alpha_{0n}^2\ p^2 - 2\ \alpha_{0n}^4\ p^4\ \eta)\}^{1/2} \qquad \text{(A13a)}$$

where

$$\mathbf{W = \{(1 + R_n - 2\ \alpha_{0n}2\ p2\ \xi_n) + [(1-R_n+2\ \alpha_{0n}2\ p2\ \xi)2-8\eta_n\ \alpha_{0n}2(1-R_n\ \alpha_{0n}2\ p2)\}1/2\}/2} \qquad \textbf{(A13b)}$$

and $\eta_n = (\varepsilon_n - \delta_n) / (R_n-1)$ and $\xi_n = R_n\ \varepsilon_n + \eta_n$.

For the quasi SV-wave

$$X(p) = \Sigma\ \{\ (\beta_{0i}^2\ p^2) / (1-\ \beta_{0i}^2\ p^2)^{1/2}\ +$$
$$\Delta_i\ ((\beta_{0i}^4\ p^4\ \omega_i + 3\ \beta_{0i}^2\ p^2 - 2) / (R_i(\beta_{0i}^2\ p^2\ \omega_i+1)^2)\} \qquad \text{(A14)}$$

where $\omega_i = 2\ \varepsilon_i / (1 - R_i)$. The exact expression for the phase incidence angle at the reflector is

$$\sin(\theta_n) = 2\ \beta_{0i}^2\ p^2 / \{\ 1 + R_i + 2\ \alpha_{0i}^2\ p^2\ \omega_n\ +$$
$$[\ (1 - R_n + 2\ \alpha_{0n}^2\ p^2\ \omega_n)^2 - 8\ \alpha_{0n}\ p\ \eta\ (1 - \beta_{0n}\ p)]1/2\} \qquad \text{(A15)}$$

The implementation given in appendix E has options for quasi P, quasi SV, SH, and P-SV converted waves. Various marine modes (PPS, PSS, PSS and PSSP) are also supported. Sources are assumed on the surface, receivers either on the surface or on the sea bottom. The layers can have transverse anisotropy (symmetry axis vertical), since this is no additional work.

Appendix B

Shear Velocity Estimation

When shear velocity is needed but not measured, it must be estimated. The usual way to do this estimation is to use an empirical relation, called a trend curve, which predicts Vs from a corresponding Vp (e.g . Castagna et. al. 1993) :

$$V_s^{TR} = V_s^{TR}(V_p) \qquad \text{(B1)}$$

For high quality shear estimation, there are two areas which must be addressed. First, the trend curve should be taken to depend on the lithology. This greatly improves the accuracy. Secondly, trend curves are normally generated for brine saturated rocks. We take these up in order.

We will work with trend curves derived from (nearly) pure lithologies, which we call end members. For mixed lithologies, one can mix the results of the end members. This, of course, assumes that you know the fraction of each lithology in the mix. These amounts are the result of a lithology analysis, discussed in the main text.

There are two basic approaches to mixing: mix the results or mix the trends. The first method just inserts the measured Vp into each end member trend, and then does some kind of average on the resulting Vs's. The other approach is to define a trend for the mixed lithology. Because the trend curves for the various lithologies do not very greatly from one another, most variants of mixing yield rather similar results.

We choose to mix the trends with an approach that can be related to theoretical mixing theories. Theories of mixing normally use the bulk and shear moduli, not the velocities. We need to estimate the densities to proceed. Fortunately, there are density / P-velocity trend curves

$$\rho^{TR} = \rho^{TR}(V_p) \qquad \text{(B2)}$$

available for various lithologies. Now we can estimate the moduli for each lithology:

$$\mu^{TR} = \rho^{TR} (V_s^{TR})^2 \qquad \text{(B3)}$$

$$K^{TR} = \rho^{TR}(V_p) V_p^2 - (4/3) \mu^{TR} \qquad \text{(B4)}$$

We could now use some theory to mix the moduli, if we knew which Vp to use for each lithology. Our strategy is to use the porosities of the end members

$$\phi^{TR} = (\rho^{TR} - \rho_{fl}) / (\rho_{ma} - \rho_{fl}) \qquad \text{(B5)}$$

We assume that each lithology has the same porosity as the overall porosity. We choose three porosities, generate the corresponding moduli for each porosity, and mix them. We also mix the porosity.

From the mixed moduli and porosities, we derive velocities. Then we fit a quadratic trend curve to the mixed shear and compressional velocities. This procedure will give back the original end member trend if there is one component of the mixture.

Note that the moduli mixing theory has not been specified. One could use e.g. the Voight-Reuss bounds, Hashin-Shtrikman bounds (see Castagna, 1993) , or Berryman's (1980) effective medium theory. Theoretically, the choice depends on the geometry of the rocks being mixed. We have coded for multiple options, but normally use the Berryman effective medium theory. It is symmetric in all components and tends toward the center of the physically allowable range.

Armed with trend curves for the mixed lithology, we proceed to estimate the shear velocity from the observer P-velocity. We do *not* assume that the observed values are for brine saturated zones. In this case the fluid must be converted to brine so that brine trend curves may be used. Our approach is similar in spirit to Greenberg and Castagna, 1992, but with some different choices in implementation.

The equations of fluid substitution are

$$K' = K + (K_f' - K_f)\,(K - K_s)^2 \,/\, \{\phi\,(K_f' - K_s)(K_f - K_s) - (K_f' - K_f)(K - K_s)\} \qquad \text{(B6a)}$$

$$\mu' = \mu \qquad \text{(B6b)}$$

$$\rho' = \rho + \phi\,(\rho_f' - \rho_f) \qquad \text{(B6c)}$$

where the primed variables are those the new state, and the unprimed variables are those of the original state (Gassmann, 1951). K and μ are the bulk and shear moduli. The ρ's are densities. The subscript f refers to the fluid, while s refers the solid grains. The moduli are related to the velocities by

$$K = \rho\,\{V_p^2 - (4/3)\,V_s^2\} \qquad \text{(B7a)}$$

$$\mu = \rho\,V_s^2 \qquad \text{(B7b)}$$

When the values of V_s, ρ, ϕ or K_s are not known from measurement, they can be estimated from empirical trend curves

$$V_s^{TR} = V_s^{TR}(V_p) \qquad \text{(B8a)}$$

$$\rho^{TR} = \rho^{TR}(V_p) \qquad \text{(B8b)}$$

$$\phi^{TR} = (\rho^{TR} - \rho_{fl}) \,/\, (\rho_{ma} - \rho_{fl}) \qquad \text{(B8c)}$$

$$\mu^{TR} = \rho^{TR} (V_s^{TR})^2 \qquad \text{(B8d)}$$

$$K_s^{TR} = \rho^{TR}(V_{p\_max})\, V_{p\_max}^2 - (4/3)\, \mu^{TR}(V_{p\_max}) \qquad \text{(B8e)}$$

for *brine* saturated rocks. If we start with brine saturated rocks, the it is easy to use the trend curves to supply unknown values. But often, we measure the V_p and ρ for a saturated zone, and want to estimate the Vs. In order to use the trend curves to estimate Vs, we must simultaneously fluid substitute from hydrocarbon to brine and use the brine trend curves. This produces a non linear system of coupled equations:

$$M' = \rho^{TR}(V_p)\, V_p^2 + (K_f' - K_f)\, \phi^{TR}(\Delta K/\phi^{TR})^2 / \{(K_f' - K_s^{TR})(K_f - K_s^{TR}) - (K_f' - K_f)(\Delta K/\phi^{TR})\} \qquad \text{(B9a)}$$

$$\Delta K(V_p) = \rho^{TR}(V_p)\, \{V_p^2 - (4/3)\, V^{TR}{}_s^2(V_p^2)\} - K_s^{TR} \qquad \text{(B9b)}$$

$$\phi^{TR}(V_p) = (\rho^{TR}(V_p) - \rho_{fl}) / (\rho_{ma} - \rho_{fl}) \qquad \text{(B9c)}$$

where M is the P-wave modulus. Equations B9 constitute the “trend consistent” fluid substitution equations.

The trend consistent equations (for reasonable trends) have the important property that The right hand side of B9a increases monotonically in V_p, over the possible range of V_p. This insures a single solution.

To be a little more specific about what constitutes “reasonable” trends, we note that If K satisfies the Voight/Reuss bounds and is concave upward in porosity and if porosity is decreasing with velocity, then it can easily be shown that monotonicity holds. While these are sufficient conditions, the necessary conditions are complex but much less restrictive.

Using measured values of ϕ, ρ or K_s, with a V_p/V_s trend curve may produce multiple solutions. The biggest problem occurs for small porosities. If the solution technique switches between branches of multiple solutions there can be a visible problem with precision, which may be more of a practical difficulty than the corresponding accuracy problem. The key to implementing this robustly is to observe that $\Delta K/\phi^{TR}$ has a finite limit as $\phi^{TR} \to 0$. After a little algebra with the trend curves, $\Delta K/\phi^{TR}$ can be coded to avoid the apparent singularity.

Often we want to use less than the full set of trend curves, because we believe that the measurements are more accurate that the values predicted by the trends. Typically, only the V_p/V_s trend curve is the only one we want to use. In such cases, we do trend consistent fluid substitution for mathematical robustness, and do corrections for the measured variations from the trend values.

The fluid substituted P-wave modulus M' can be viewed as a function of the original velocities and density, porosity, grain modulus and both fluid moduli:

$$M' = \rho'(V_p')^2 = F(V_p,V_s,\rho,\phi,K_s; K_f',K_f) \qquad \text{(B10)}$$

For small deviations from the trends, we can expand

$$M' = F(V_{p0},V_s^{TR}(V_{p0}),\rho^{TR}(V_{p0}),\phi^{TR}(V_{p0}),K_s^{TR}; K_f',K_f) +$$

$$\delta F/\delta V_p\,(V_p - V_{p0}) + \delta F/\delta Vs\,(V_s - Vs^{TR}(V_{p0})) +$$

$$\delta F/\delta\rho\,(\rho - \rho^{TR}(V_{p0})) + \delta F/\delta\phi\,(\phi - \phi^{TR}(V_{p0})) +$$

$$\delta F/\delta K_s\,(K_s - K_s^{TR}(V_{p0}))$$

neglecting higher order derivatives. Choosing V_{p0} so that

$$M' = F(V_{p0},V_s^{TR}(V_{p0}),\rho^{TR}(V_{p0}),\phi^{TR}(V_{p0}),K_s^{TR}; K_f',K_f)$$

gives the fully trend consistent solution V_{p0}. Then we can estimate the change caused by deviations from the trends

$$Vp = Vp0 - (\delta F/\delta Vp)^{-1}\{\delta F/\delta Vs(V_s - V_s^{TR}(V_{p0})) + \delta F/\delta\rho\,(\rho - \rho^{TR}(V_{p0})) + \delta F/\delta\phi\,(\phi - \phi^{TR}(V_{p0})) + \delta F/\delta K_s\,(K_s - K_s^{TR})\}$$

where the partial derivatives are evaluated along the trends. If there is no measured data for any term in the correction formula, just drop that term, which is equivalent to accepting the trend curve value for that parameter.

Part III

High Resolution Processing of the Gypsy Hugh Resolution 3D Seismic Data

by

Carlos Moreno, Roger Young, John Castagna

Our first attempt to use the Gypsy 3D seismic data in a quantitative sense revealed inadequacies in the original processing. These data were reprocessed at the University of Oklahoma in the Shell Crustal Imaging Facility directed by Dr. Roger A. Young and led to a paper submitted to the annual convention of the Society of Exploration Geophysicists presented by Carlos Moreno. The paper is herein attached as Part III of this report.

Appropriate Acquisition and Processing for Shallow 3-D Seismic Surveys

Carlos E. Moreno*, Roger Adams Young, John P. Castagna,
The University of Oklahoma, Norman, OK

Summary

A conventionally processed, high-resolution 3-D seismic survey at the OU Gypsy test site exhibited poor ties to well control. The data was reprocessed with surface consistent predictive deconvolution, muting of wide-angle reflections, min/max exclusion stacking, and F-XY deconvolution. After reprocessing, a good character match with synthetic seismograms was observed.

Introduction

3-D seismic reflection surveys targeting features at depths of 1000 ft or less are commonly acquired nowadays. Many of these surveys are part of oil exploration or development programs by smaller energy industry companies and contractors, but the use of 3-D surveys outside the energy industry is also growing (eg., Villella et al., 1997; Siahkoohi and West, 1998). The vast experience of the energy industry in acquisition and processing 3-D surveys provides a wealth of guidance for those less familiar with 3-D methods. However, relying on acquisition parameters and processing approaches designed for deeper targets may have its pitfalls. In the most unfavorable case, a survey may be both over-designed and unsuited for shallow imaging. A choice of processing parameters typical of deeper targets may also lead to a poor stack of shallow targets.

This paper shows how processing appropriate to shallow targets can produce a favorable image that greatly improves the tie with a zero-offset synthetic trace. It concludes with some suggestions about reprocessing the shallow reflections contained within data originally acquired with deeper objectives in mind.

Survey acquisition

Figure 1 shows the location of the Gypsy Project Subsurface study site NW of Tulsa, OK. This site was chosen by BP Petroleum for characterizing a clastic reservoir interval by borehole and surface geological and geophysical methods (Doyle and Sweet, 1995). A nearby outcrop study site afforded geological mapping and physical property measurements of the same units encountered at the subsurface site at a depth of approximately 1000 ft. The Gypsy database and the site itself were ceded to the University of Oklahoma by BP in 1994.

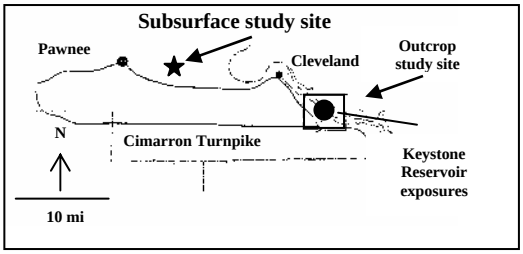

Figure 1 Location of the Gypsy study sites

The 3-D seismic survey at the Subsurface study site (Figure 2) was small in area, covering approximately 0.16 km^2 (40 acres).

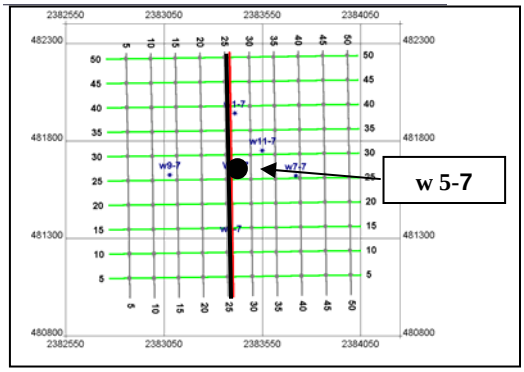

Figure 2 Survey basemap, inline 26, and well 5-7.

Recording parameters and acquisition geometry are given in Tables 1 and 2, respectively.

RECORDING	PARAMETERS
Recorded by	Western Geophysical
Date	Jan. 1990
Recording system	MDS-16
Format	SEG-B
Geophone type	LRS 1011 (28 Hz)
Filter	9-250 Hz
Notch filter	Out
Sample rate	1 ms
Record length	3000 ms
Bin size	25 ft by 25 ft

Table 1 Recording parameters for the 3-D survey

ACQUISITION	GEOMETRY
Energy source	Dynamite
Source pattern	Single charge (1 lb/shot)
	Shot depth 90, 100, 110, 120 ft (same hole, 3 times)
Shot interval	~140 ft
Number of shot lines	7 (45 deg to receivers)
Shot line separation	~250 ft
Shots per swath	40
Number of swaths	3
Receiver interval	50 ft (N-S)
Receiver line spacing	50 ft (E-W)
Receiver lines/shot	9 (every 150 ft)
Channels per rcv. line	27: *27x9=143* live ch/sht
Crossline line roll	1 receiver line (50 ft)
Inline line roll	0 (no movement N-S)
Geophones/station	12
Geophone array	25 ft circle

Table 2 Acquisition parameters for the 3-D survey

Standard Processing

The 3-D processing flow in this paper is chosen to image the shallow targets at times of 250 ms or less in the upper part of the data acquired. Two sequences of processing steps were applied to the 3-D data using ProMAX 3D. **Standard processing** (Table 3, top) included binning, amplitude recovery, trace editing, and statics correction. Nominal fold for inner bins exceeded 50, but the 70 % stretch mute limited the offset range in stacking very shallow events. Figure 3 shows that the effective fold for events at times less than 200 ms is approximately 10 or less. In the Gypsy interval at approximately 250 ms, however, the fold is nearly half the nominal fold. An upper datum was adopted, and residual statics was accomplished in a 3-D sense. Figure 4a shows inline 26 through residual statics.

STANDARD	PROCESSING
1.Geometry; binning	
2.True amp. recovery	a^{-2}, a=1.5
3.Trace editing	
4.Trace shortening	Reduce to 1 s
5. Datum statics correction	Final datum: 1000 ft
6. Resid. statics correction	
7. Resid. statics correction	
APPROPRIATE	**PROCESSING**
8. Bandpass filtering	35-45-250-400
9. Sur. con. pre. decon.	Op. Len.: 10 ms
	Win. Len.: 200 ms
10. NMO correction	Stretch mute: 70%
11. Angle-limited muting	Max. angle:~30 deg
12. Min/max excl stacking	
13. F-XY decon.	5 by 5 traces

Table 3 Processing steps

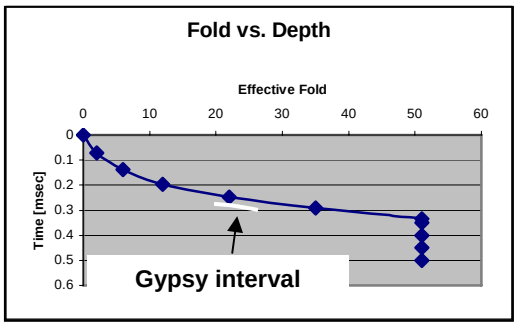

Figure 3 Fold decreases with depth due to the processing stretch mute.

Appropriate processing

Appropriate processing began with the result from standard processing and applied additional steps that take into account the special requirements of the shallow reflections. Table 3 (bottom) shows the steps in appropriate processing that were chosen after extensive parameter testing. These consist of bandpass filtering, surface consistent predictive deconvolution, angle-limited muting, minimum/maximum exclusion stacking, and F-XY deconvolution.

Bandpass filtering Figure 4b shows inline 26 through bandpass filtering (35-45-250-400). This filter is, essentially, a lowcut filter as spectra show that the highest frequency of the seismic data is less than 250 Hz. The improvement is due mainly to the attenuation of the groundroll, which has high-frequency modes that overlap the frequency band of reflections (Liu, 1999). The loss of reflection amplitude in this band is, of course, unfortunate and will affect the stack, but the improvement in S/N (Figure 4b, boxes) justifies the step.

Surface consistent predictive deconvolution
Pre-stack surface consistent deconvolution not only increased noticeably the S/N ratio, it also improved the frequency bandwidth (Figure 4b and c, boxes), which would be important for a detailed interpretation.

Angle-limited mute Comparison of the synthetic trace (Figure 4, between panels) to the processing result through predictive deconvolution (Figure 4c) shows that there is a relatively good match between the two for times greater than 120 ms. It is clear, however, that the strongest events on the synthetic trace do not correspond to the strongest events in the stacked data. In particular, a strong, stacked event at approximately 185 ms (Figure 4c, arrow) does

not appear to have an equivalent on the synthetic trace. This lack of correspondence raises several questions. Is the log depth-to-time conversion inaccurate? Did the logging tool function properly? Is the seismic wavefield seeing the impedance changes shown by the sonic log?

An exhaustive analysis of the logs indicates that for a given depth the time difference is less than 6 ms suggesting that the depth-to time curves are not the problem. Very careful editing of the logs has reduced the possibility of an anomolous impedance response. The presence of many events in the seismic data suggests that the seismic wavefield is, in fact, responding to impedance changes. This situation led us to question a fundamental assumption that is made in comparing the synthetic trace and the stacked section, namely, that the stacked trace is equivalent to a zero-offset trace. This may not be valid when data is stacked over a range of incidence angles because both amplitude and phase vary with angle. The result may be that the stacked event is not similar to the synthetic event.

In order to establish the range of incidence angles present in the binned gathers after stretch muting, CMP ray tracing was performed. These results were used to construct an angle-limited mute pattern. Figure 4d shows the stack after muting traces with angles of incidence exceeding approximately 30 deg. The stack corresponds much more favorably at 185 ms (Figure 4d, arrow) with the synthetic trace once the wide-angle reflections are eliminated from the stack.

Min/max exclusion stacking Both a mean stack and a non-conventional stack, the minimum/maximum exclusion method, were tested. The advantage of the latter is that it excludes anomalous values, and it drops null values due to muting. Figure 5 shows the two stacks after F-XY deconvolution. In order to equalize amplitudes, AGC was applied to gathers just before mean stack using a 1,000 ms window to preserve trace-to-trace amplitudes. Shallow events (solid box) are weaker than deeper events (dashed box) on the mean stack (Figure 5b, right) because muting is greater for shallower traces. The minimum/maximum exclusion method (Figure 5b, left), on the other hand, shows a much more uniform amplitude distribution for both shallow and deep events (Figure 5a: solid and dashed boxes, respectively).

F-XY deconvolution A final step, F-XY deconvolution, is applied in order to attenuate random noise remaining after stack.

Conclusions

3-D reflection processing requires additional steps to account for the special properties of shallow reflections. These steps may include bandpass filtering, predictive deconvolution, angle-limited muting, and min/max stacking, which take into account the overlap in signal and noise and the very wide range of incident angles at reflectors. A much better match between a zero-offset synthetic trace and the stacked section results if appropriate processing is used to attenuate residual groundroll, to improve the bandwidth of the data, to mute wide-angle reflections, and to drop from the stack null values resulting from muting.

When considering a reprocessing of 3-D data to enhance shallow reflections, a ray trace analysis using an approximate interval velocity model is important to establish the range of incidence angles expected for the shallow target horizons. Excluding the widest angles from the stack may be necessary to obtain a tie with well data.

Acknowledgments

The authors are grateful to the Gypsy Project, Institute for Reservoir Characterization, and the Institute for Exploration and Development Geosciences, Univ. of Oklahoma, for use of geophysical data, and to Bill Lamb for assistance in editing the log data. Financial support was provided by PDVSA and the OU Geophysical Reservoir Characterization Consortium.

References

Villella, A. C., Xia, J. and Miller, R. D., 1997, Delineation of salt dissolution sinkholes using minimal deployment shallow 3-D seismic reflection surveying: Annual Meeting Abstracts, Society Of Exploration Geophysicists, 780-783.

Siahkoohi, H. R. and West, G. F., 1998, 3-D seismic imaging of complex structures in glacial deposits: Geophysics, 63, no. 03, 1041-1052.

Doyle, J.D., Sweet, M.L., 1995, Three-dimensional distribution of lithofacies, bounding surfaces, porosity, and permeability in a fluvial sandstone-Gypsy Sandstone of Northern Oklahoma, AAPG Bulletin, 70, 70-80.

Liu, Z.-M., 1999, Methods of velocity determination and noise reduction in the processing of near-surface seismic reflection data, unpublished Ph.D. thesis, Univ. of Oklahoma, 186 pp.

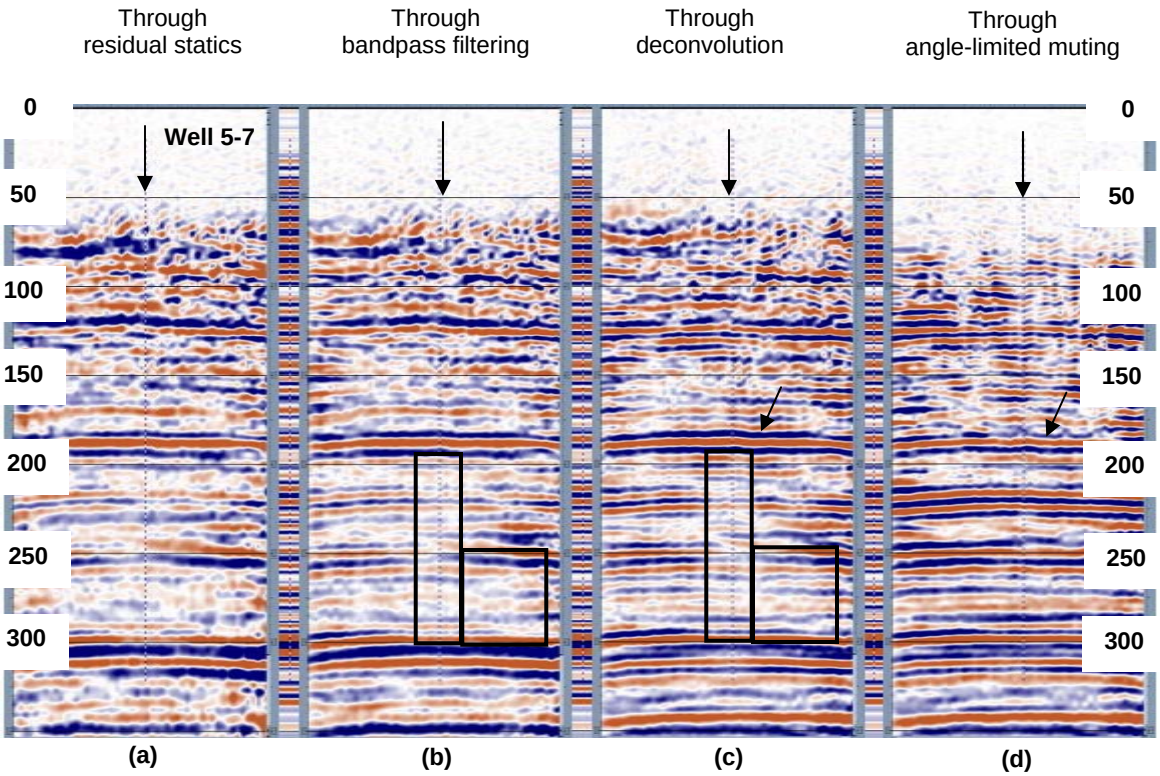

Figure 4 Processing stages: Standard processing (a). Appropriate processing (b-d). All sections are displayed with F-XY deconvolution. Small panels between sections are the zero-offset synthetic trace.

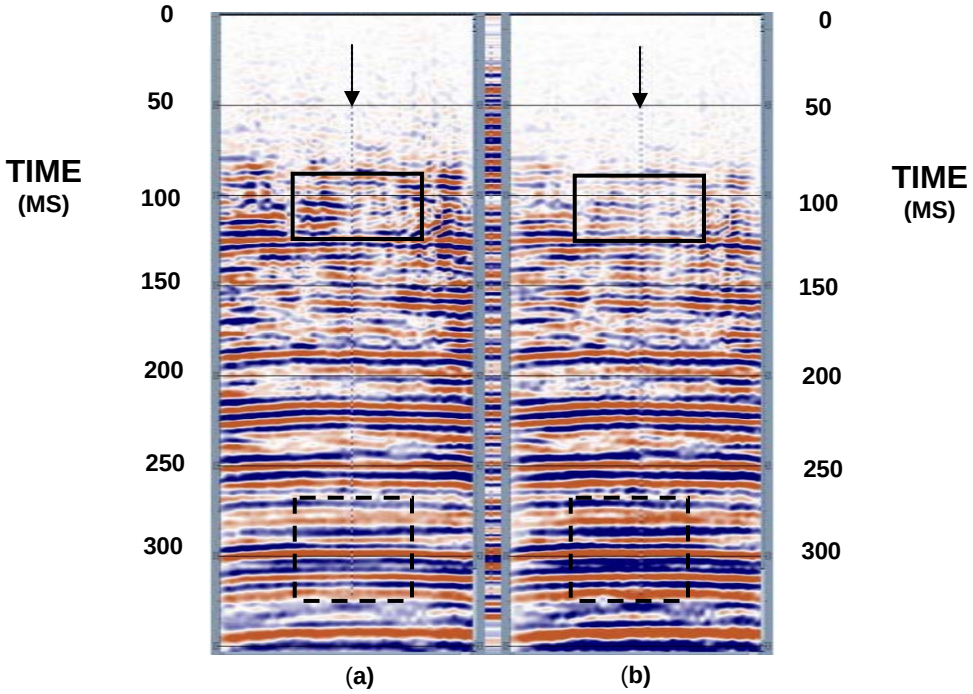

Figure 5 Stacking by (a) the minimum/maximum exclusion method; (b) the mean stack method. Both sections are displayed with F-XY deconvolution.

Part IV

On the Use of Gypsy Field Data in Reservoir Characterization Education at the University of Oklahoma

by

Lynn Soreghan

The Gypsy Field data has been used to change the way we teach reservoir characterization and sedimentary geology at the University of Oklahoma. Included in this report is an abstract for a paper presented at the Geological Society of America annual meeting describing our efforts in this regard. Also included is a hardcopy of the website for my sedimentary geology course.

THE USE OF CASE STUDIES TO EXPAND THE RELEVANCE OF SEDIMENTARY GEOLOGY FOR FUTURE GEOSCIENTISTS

SOREGHAN, Gerilyn S., and SOREGHAN, Michael J., School of Geology and Geophysics, University of Oklahoma, Norman, OK, 73069.

We are restructuring our sedimentary geology course to highlight the broad application of sedimentary geology and enhance the relevance of the material for future geoscientists. Our primary goals are to: 1) produce geoscience graduates with broad competence in the many applications of sedimentary geology, 2) shift from a "topical roll call" approach that emphasizes classification and memorization skills to a problem-solving approach that emphasizes critical thinking and communication skills, and 3) produce a model with web-based and hardcopy materials that can be adopted at other institutions. We aim not to achieve an exhaustive coverage of the multitude of material encompassed in typical sedimentary geology courses, but to cover fundamental and selected concepts in the context of the large array of problems to which sedimentary geology is applicable.

Upon completion of the restructuring, we will divide the course into several modules representing fundamental and applied case studies in sedimentary geology. Following introductory materials on fundamental concepts, present and future modules cover aspects of basin analysis, reservoir characterization, environmental geology, natural hazards and global change. The case studies utilize real data from academic, governmental and industrial sources. Background and supplemental data for some of the case studies are presently available to students through a series of web pages designed for the course. Student teams complete each module and make and present detailed recommendations or interpretations based on the available data. Class time is not divided into lab and lecture; instead class time includes student group work, laboratory analyses, topical seminars, field work and instructor and student-led discussions

This is the first semester in which we are attempting most of these changes, and therefore we do not have summative results. Both student and peer evaluations prior, during and after full implementation will provide a measure of the effectiveness of our approach. Industrial recruiters will evaluate selected case studies and will participate in evaluation of student-team presentations. Upon completion we will request instructors from other institutions to evaluate the case studies.

Education, case-study, sedimentary geology

Presented at Geological Society of American Annual Meeting.